



A Hierarchical Control Approach for Power Loss Minimization and Optimal Power Flow within a Meshed DC Microgrid

Igyso Zafeiratou, Ionela Prodan, Laurent Lefèvre

► To cite this version:

Igyso Zafeiratou, Ionela Prodan, Laurent Lefèvre. A Hierarchical Control Approach for Power Loss Minimization and Optimal Power Flow within a Meshed DC Microgrid. *Energies*, 2021, 14 (16), pp.4846. 10.3390/en14164846 . hal-04030339

HAL Id: hal-04030339



<https://hal.science/hal-04030339>

Submitted on 15 Mar 2023

HAL is a multi-disciplinary open access archive for the deposit and dissemination of scientific research documents, whether they are published or not. The documents may come from teaching and research institutions in France or abroad, or from public or private research centers.

L'archive ouverte pluridisciplinaire **HAL**, est destinée au dépôt et à la diffusion de documents scientifiques de niveau recherche, publiés ou non, émanant des établissements d'enseignement et de recherche français ou étrangers, des laboratoires publics ou privés.

A hierarchical control approach for power loss minimization and optimal power flow within a meshed DC microgrid

Igyso Zafeiratou ¹, Ionela Prodan ¹  0000-0002-3522-5192 and Laurent Lefèvre ¹  0000-0002-5496-5882

¹ Univ. Grenoble Alpes, Grenoble INP⁰, LCIS, F-26000 Valence, France

* Correspondence: igyso.zafeiratou@gmail.com

Abstract: This paper considers the DC part of a hybrid AC/DC microgrid with a meshed topology. We address cost minimization, battery scheduling and the power loss minimization within the power distribution network through constrained optimization. The novelty comes from applying differential flatness properties to the microgrid components and formulating the cost and constraints in terms of the associated B-splines parametrization of the flat outputs (the voltages and currents of the system). This allows us to obtain optimal power profiles which ensure the minimization of the DC-bus power loss and the electricity cost. These profiles are tracked by a model predictive controller at the higher level, while the low level controller handles the switching operations within the DC/DC converters. Extensive simulations under nominal and fault-affected scenarios using realistic data validate the proposed approach.

Keywords: DC microgrid architecture, Meshed topology, Power dissipation, Load balancing, Differential flatness, B-spline parametrization, Model Predictive Control (MPC).

1. Introduction

Microgrids are complex power systems and their efficient operation demands the study on multiple interlocking factors, such as power losses, electricity cost, renewable resources, component size and the like. To date, the state of the art in the microgrid topic has shown promising results in the power flow amelioration and performance enhancement [1]. Optimal power flow accounts for the effective and reliable functioning of the system by either minimizing the electricity cost or the energy dissipation. The existence of power loss in the transmission-line network can significantly affect the power quality during distribution. Hence, the power loss mitigation is a very important factor and leads towards the improvement of the power transmission [2].

Several approaches have been considered recently for the power loss minimization, emphasizing either the components linked to the microgrid or the transmission network [3]. Some researchers, as in [4] and [5], concentrate on the network's topology or the planning of the renewable sources and the energy storage (ES). Others concentrate on the existing power losses in the transmission lines, which are inherent to the electrical network and which cannot be prevented or eliminated [6]. In the literature, researchers have proposed several methods for optimal power distribution including power loss minimization. In [7], a three-layer hierarchical control strategy is proposed to handle the energy management in islanded microgrids. More specifically, at the higher level, taking into account topological and stability issues, optimal power profiles are generated, within a MPC framework. At the middle level, using the upper level references, a voltage regulation problem is solved taking into account the power losses of the transmission network and the converters. Furthermore, a two-level hierarchical control based on plug and play method has been proposed in [8] where at a low level load sharing is achieved through droop control and at a higher level adaptive droop controllers are developed

Citation: Zafeiratou, I.; Prodan, I.; Lefèvre, L. Title. *Journal Not Specified* **2021**, *1*, 0. <https://doi.org/>

Received:

Accepted:

Published:

Publisher's Note: MDPI stays neutral with regard to jurisdictional claims in published maps and institutional affiliations.

Copyright: © 2021 by the authors. Submitted to *Journal Not Specified* for possible open access publication under the terms and conditions of the Creative Commons Attribution (CC BY) license (<https://creativecommons.org/licenses/by/4.0/>).

⁰ Institute of Engineering Univ. Grenoble Alpes

for power losses minimization. [9] introduces an optimal power flow algorithm for islanded microgrids to cope with central power dissipation under a centralized three-layer supervision controller.

Contributions: In [10], the complete three-layer hierarchical control strategy was presented. A constrained optimization-based problem for power balancing and cost minimization was implemented without considering the power losses in the transmission lines of the central network. In this work we focus on the enhancement of the optimization problem, in particular for the high level where we account for the power losses in the transmission lines. The contributions are summarized below:

- power loss mitigation within the central transmission network is considered in the optimization problem to improve the power flow routing while at the same time the electricity cost is taken into account. The formulation of the high level optimization problem is done through the analytical computation of the system's flat representation together with B-spline parametrization;
- detailed model description of the central power dissipation to represent the transmission lines including voltage drops among the connecting nodes¹. Supplementary constraints are considered to maintain the voltage in the DC network close to the nominal value of 400 V;
- verification of the meshed topology of the central network in the case of unexpected events (e.g. blackouts). The validation of the approach is done through extensive simulations considering different scenarios in the central transmission network.

Note that the cost function and the constraints will be posed in a flat representation (rewritten in terms of a flat output and its derivatives). Further parametrizing the flat output by a family of B-spline functions will allow to check continuous time constraints through a finite number of decision variables (the control points defining the B-spline parametrization). More details on the concepts of flatness and B-spline parametrization can be found in [11], [12], [13].

Outline: Section 2 concerns the abbreviations. In section 3 a brief description of the ES (Energy Storage) dynamics is introduced and the detailed model of the central transmission network are introduced. Section 4 contains the multilevel hierarchical control problem, with the high and the middle levels being detailed in particular. Section 5 presents the simulation results and section 6 provides the conclusions and the future work.

¹ A connecting node is the point where a source or a load is linked to the central network as in Fig. 1 below for the points 1, 2, 3, 4.

2. Notations

ES, es	energy storage system
UG, ug	utility grid
PV, pv	solar panel system
$DERs$	distributed energy resources
$x(t)$	state vector of the system $\in R^n$
$u(t)$	input vector of the system $\in R^m$
$y(t)$	output vector of the system $\in R^m$
$KiBaM$	Kinetic Battery Model
P	electrical power
Sw	switches of the Split–Pi converter
d_{1sc}	duty cycle which for Sw_4 is $1-d_{1sc}$ and Sw_3 is d_{1sc}
d_{2sc}	duty cycle which for Sw_1 is $1-d_{2sc}$ and Sw_2 is d_{2sc}
q_{1b}	available charge state of the KiBaM battery
q_{2b}	bound charge state of the KiBaM battery
b	KiBaM battery
sc	Split–Pi Converter
C	capacitor
I	inductor
R_{1b}	resistance between the KiBaM battery and the Split–Pi converter
R_{2b}	resistance of the KiBaM battery
R_1, R_2, R_3, R_4	resistances of the transmission network
R_{1sc}	resistance among the DC network and the Split–Pi converters
i_{sc_out}	output current of the Split–Pi converter
v_{sc_out}	output voltage of the Split–Pi converter
i_{sc_in}	input current of the Split–Pi converter
v_{sc_in}	input voltage of the Split–Pi converter
r	derivative of the B-spline
p_i	i^{th} control point
$b_{i,d}$	i^{th} B-spline of order d
$\mathcal{B}(t)$	vector of the B-splines $\in R^{d \times N}$
\mathcal{P}	vector of control points $\in R^{3 \times N}$
$\mathcal{S}_{\kappa,d-r,d}$	translation matrix from higher to lower degree basis functions
$\mathcal{M}_{d,d-r}$	matrix performing the linear combinations of the lower-degree basis functions
T	knot vector $\in R^{N+d}$
τ_κ	κ^{th} knot
κ	number of knots
e	electricity price
$Q_{\tilde{y}}, R_{\tilde{u}}$	weight matrices

3. DC microgrid model description

The DC microgrid, part of a hybrid AC/DC architecture with a meshed topology (Fig. 1), also described in [10], is composed by a set of DS–100 PVs (180 W peak PV generation), an ES with a set of AGM 12–165 lead acid batteries (165 Ah battery capacity with a discharge rate of 20 hours at 25°C) and a consumer load (3901 W peak demand). These components are linked to the central transmission network (around 400 V DC) through a particular type of DC/DC converters: Split-Pi converters, which regulate the input/output voltage from and towards the sources and the loads. The DC microgrid is connected to the UG through an AC/DC converter. In this work, we focus on the detailed analysis of the DC central transmission network and the ES system (Split-Pi

converter connected to the battery). However, the following approach can be similarly applied for the primarily proposed design in [14]. The overall hybrid AC/DC grid contains an AC/DC converter, placed between the grid and the DC microgrid (Fig. 1), where supplementary buses (AC or DC) or sources (AC or DC) could be included, since a meshed topology of a multiple-line transmission network is considered. However, for an AC/DC converter, an AC bus or an AC source, the characteristics of the AC power should be taken into account, such as the active power, the reactive power, the frequency and the like [15].

This section builds upon our previous paper [10], where the mathematical model of the ES system was explicitly introduced. In this work, we will continue with the explicit description of the dynamics of the central transmission network, since the power losses are now considered and resistors exist to replace every transmission line. The mathematical methodology employed relies upon the port-Hamiltonian (PH) formalism [16]. This method provides an explicit description of the routing elements (inductors, capacitors, resistors) existing in the electrical network. An advantage of this method is that the set of equations can be directly derived by the associated Bond Graph of the electrical system [17,18], which is a graph-oriented modeling tool for the dynamics of convoluted physical systems. Detailed information and analysis on the modeling methodology is available in [14] and [10].

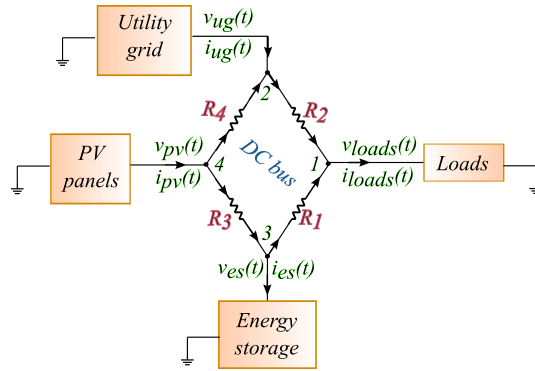


Figure 1. Central electrical network of the meshed DC microgrid system under the existence of power losses.

3.1. Brief description of the ES subsystem

The ES system (Fig. 2) contains a lead acid battery connected to a Split-Pi converter. The circuit of the battery is structured according to the Kinetic Battery Model (KiBaM), composed by two capacitors linked together with a resistance. The charges of the capacitors represent the total charge of the battery. Furthermore, the Split-Pi converter is a bidirectional buck-boost converter which regulates the voltage in both directions. The

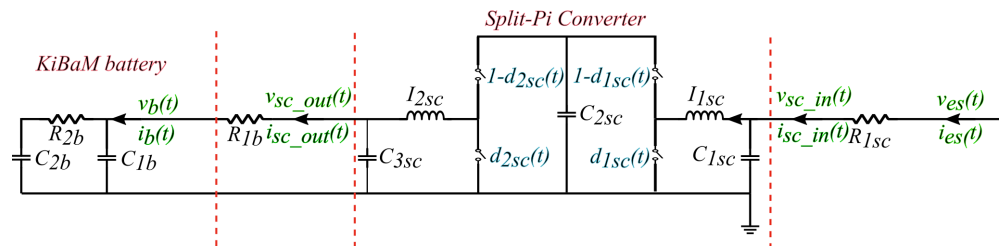


Figure 2. Electrical circuit of ES, where the input voltage v_{es} is equivalent to the voltage entering from the central transmission network v_{DC} .

state-space representation of the ES system was already explicitly presented in [10] and arrives, after various computations, to the nonlinear state-space mathematical model:

$$\dot{p}_{1sc}(t) = \frac{q_{1sc}(t)}{C_{1sc}} - \frac{q_{2sc}(t)}{C_{2sc}}(1 - d_{1sc}(t)), \quad (1a)$$

$$\dot{p}_{2sc}(t) = \frac{q_{2sc}(t)}{C_{2sc}}(1 - d_{2sc}(t)) - \frac{q_{3sc}(t)}{C_{3sc}}, \quad (1b)$$

$$\dot{q}_{1sc}(t) = \frac{v_s}{R_{1sc}} - \frac{q_{1sc}(t)}{C_{2sc}R_{1sc}} - \frac{p_{1sc}(t)}{I_{1sc}}, \quad (1c)$$

$$\dot{q}_{2sc}(t) = \frac{p_{1sc}(t)}{I_{1sc}}(1 - d_{1sc}(t)) - \frac{p_{2sc}(t)}{I_{2sc}}(1 - d_{2sc}(t)), \quad (1d)$$

$$\dot{q}_{3sc}(t) = \frac{p_{2sc}(t)}{I_{2sc}} - i_{R_{1b}}(t), \quad (1e)$$

$$\dot{q}_{1b}(t) = i_{R_{1b}}(t) - \frac{q_{1b}(t)}{C_{1b}R_{2b}} + \frac{q_{2b}(t)}{C_{2b}R_{2b}}, \quad (1f)$$

$$\dot{q}_{2b}(t) = \frac{q_{1b}(t)}{C_{1b}R_{2b}} - \frac{q_{2b}(t)}{C_{2b}R_{2b}}. \quad (1g)$$

The p variables correspond to the magnetic flux of the inductors and q to the charges of the capacitors. I_{1sc} , I_{2sc} , C_{1sc} , C_{2sc} , C_{3sc} , C_{1b} , C_{2b} are the circuit's parameters, where I is the inductance and C is the capacitance. The state vector of the system is $x_{es}(t) = [p_{1sc}(t) \ p_{2sc}(t) \ q_{1sc}(t) \ q_{2sc}(t) \ q_{3sc}(t) \ q_{1b}(t) \ q_{2b}(t)]^T \in R^{7 \times 1}$, the input vector is $u_{es}(t) = [-v_{DC}(t) \ -i_{R_{1b}}(t)]^T \in R^{2 \times 1}$ and the output vector is $y_{es}(t) = [i_{DC}(t) \ v_{R_{1b}}(t)]^T \in R^{1 \times 2}$, where $i_{DC}(t)$ is the current during charging mode. Furthermore, from the ES circuit in Fig. 2 and [10], the following relations will prove useful for the control design stage:

$$i_b(t) = i_{R_{1b}}(t), \quad (2a)$$

$$v_b(t) = \frac{q_{1b}(t)}{C_{1b}}, \quad (2b)$$

where $i_{R_{1b}}$ is the current of the R_{1b} resistor, q_{1b} is the charge of the C_{1b} capacitor and C_{1b} is its corresponding capacitance. Taking into account that the Split-Pi converter is ideal, the input power of the converter, $P_{sc_in}(t)$, is equal to the output power of the converter, $P_{sc_out}(t)$ leading to:

$$v_{sc_in} \cdot i_{sc_in} = v_{sc_out} \cdot i_{sc_out}. \quad (3)$$

Additionally, through Ohm's law, a connection among the input and output voltage, $v_{sc_in}(t)$ and $v_{sc_out}(t)$ and current, $i_{sc_in}(t)$ and $i_{sc_out}(t)$, of the Split-Pi converter and the input voltage, $v_{es}(t)$, and current, $i_{es}(t)$, of the ES system and the input voltage, $v_b(t)$, and current, $i_b(t)$, of the battery are obtained below:

$$v_{sc_in}(t) = v_{es}(t) - R_{1sc}i_{es}(t) \quad (4a)$$

$$v_{sc_out}(t) = v_b(t) + i_b(t)R_{1b} \quad (4b)$$

$$i_{sc_in}(t) = i_{es}(t) \quad (4c)$$

$$i_{sc_out}(t) = i_b(t) \quad (4d)$$

Therefore, combining the above equations in (4) and in (7), we conclude to the relations below:

$$v_{es}(t) = \frac{v_b(t) + i_b(t)R_{1b}}{\alpha(t)} + R_{1sc}\alpha(t)i_b(t) \quad (5a)$$

$$i_{es}(t) = \alpha(t)i_b(t) \quad (5b)$$

and the ES power is deduced as follows:

$$P_{es}(t) = v_{es}(t)i_{es}(t) = (v_b(t) + i_b(t)R_{1b})i_b(t) + R_{1sc}(\alpha(t)i_b(t))^2 \quad (6)$$

The duty cycles, $d_{1sc}(t)$ and $d_{2sc}(t)$, enable the operation of the converter within the ES system, ($d_{1sc}(t)$ for switches Sw_{1sc} and Sw_{2sc} and $d_{2sc}(t)$ for switches Sw_{3sc} and Sw_{4sc}). The high-voltage DC-bus of the microgrid constrains the Split-Pi converter's operation in down-conversion towards the power sources and up-conversion towards the central transmission network [10]. Thus, $d_{1sc}(t)$ will be always 0 and $d_{2sc}(t) \in (0, 1)$. Hence, according also to [19], the following was proved:

$$\alpha(t) = 1 - d_{2sc}(t), \quad (7)$$

with the α factor, a parameter chosen to be equal to $\alpha(t) = \frac{1 - d_{2sc}(t)}{1 - d_{1sc}(t)}$, showing the link between the two duty cycles of the Split-Pi converter.

105 3.2. Dynamical representation of the DC bus

The dynamical model of the four-line transmission network (Fig. 1) is developed by its Bond graph as already explained in [14]. [14] provides the Bond graph of the central transmission network taking into account each transmission lines as an RL circuit². In this work, the central network is further simplified eliminating the inductors. In DC networks, the existence of the inductors is necessary only when the current flow of the system varies. But once the system comes to its steady state, where the current flow remains stable, the inductors have no effect in the DC networks. Hence, each transmission line will be considered as a resistor and the power conservation equation is as follows (Fig. 1):

$$P_{ug}(t) + P_{pv}(t) - P_{es}(t) - P_{loads}(t) - P_{R1}(t) - P_{R2}(t) - P_{R3}(t) - P_{R4}(t) = 0, \quad (8)$$

where $P_{ug,pv,es,loads}$ is the power of the sources and the loads, while $P_{R1,R2,R3,R4}$ is the power loss for each line. The correspondingly-modified Bond graph of the central DC bus is depicted in Fig. 3.

Hence, from the the Bond graph in Fig. 3, where only dissipative elements are included, the following is obtained:

$$\begin{bmatrix} i_{pv} \\ i_{ug} \\ i_{es} \\ i_{loads} \end{bmatrix} = \begin{bmatrix} \frac{1}{R_3} + \frac{1}{R_4} & -\frac{1}{R_4} & -\frac{1}{R_3} & 0 \\ \frac{1}{R_4} & -\frac{1}{R_4} - \frac{1}{R_2} & 0 & \frac{1}{R_2} \\ \frac{1}{R_3} & 0 & -\frac{1}{R_3} - \frac{1}{R_1} & \frac{1}{R_1} \\ 0 & \frac{1}{R_2} & \frac{1}{R_1} & -\frac{1}{R_1} - \frac{1}{R_2} \end{bmatrix} \begin{bmatrix} v_{pv} \\ v_{ug} \\ v_{es} \\ v_{loads} \end{bmatrix}. \quad (9)$$

110 Therefore, from the above mentioned equations, the current flows will be deduced as follows:

- from node 1:

$$i_{loads} = i_{R1} + i_{R2} = \frac{v_{es} - v_{loads}}{R_1} + \frac{v_{ug} - v_{loads}}{R_2}; \quad (10)$$

- from node 2:

$$i_{es} = i_{R3} - i_{R1} = \frac{v_{pv} - v_{es}}{R_3} - \frac{v_{es} - v_{loads}}{R_1}; \quad (11)$$

² It is a circuit with a resistor and an inductor in series.

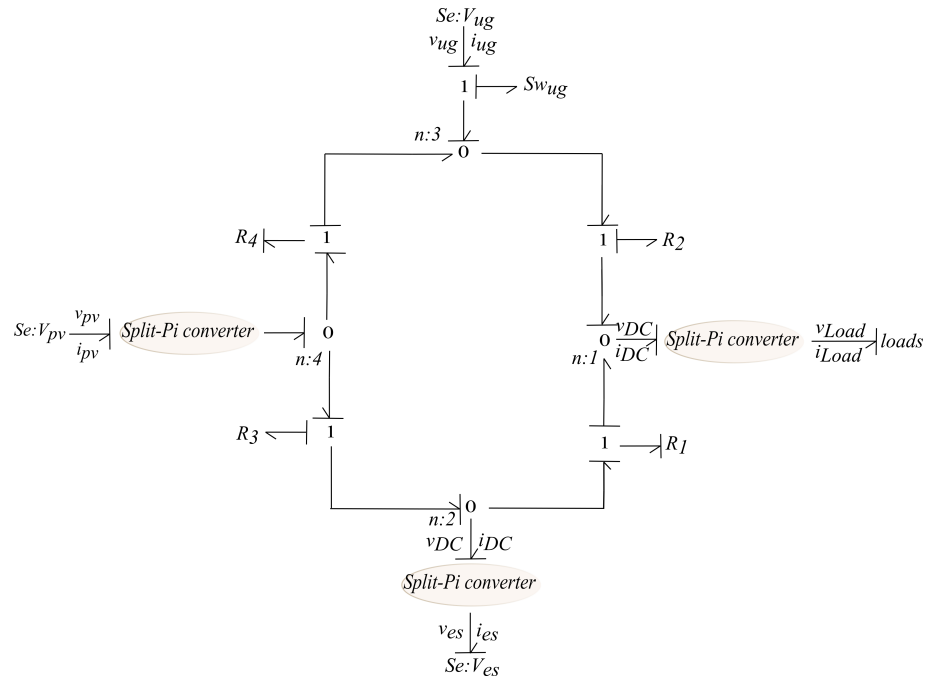


Figure 3. Bond graph of the DC micgrid's central transmission network with resistors replacing the transmission lines.

- from node 3:

$$i_{ug} = i_{R_4} - i_{R_2} = \frac{v_{pv} - v_{ug}}{R_4} - \frac{v_{ug} - v_{loads}}{R_2}; \quad (12)$$

- from node 4:

$$i_{pv} = i_{R_3} - i_{R_4} = \frac{v_{pv}(t) - v_{es}(t)}{R_3} - \frac{v_{ug}(t) - v_{pv}(t)}{R_4}. \quad (13)$$

The goal is to express all the powers appearing in the grid in terms of voltages and resistances (i.e., to avoid the explicit appearance of currents). Through (10), (11), (12), (13) we make use of the fact that the power in every electrical element is $P = i \times v$. Hence, every power variable of the DC network is expressed below in function of the voltages on the connecting nodes:

$$P_{ug} = v_{ug} i_{ug} = v_{ug} [i_{R_4} - i_{R_2}] = v_{ug} \left[\frac{v_{ug} - v_{pv}}{R_4} - \frac{v_{loads} - v_{ug}}{R_2} \right] \quad (14a)$$

$$P_{es} = v_{es} i_{es} = v_{es} [i_{R_3} - i_{R_1}] = v_{es} \left[\frac{v_{pv} - v_{es}}{R_3} - \frac{v_{es} - v_{loads}}{R_1} \right] \quad (14b)$$

$$P_{pv} = v_{pv} i_{pv} = v_{pv} [i_{R_3} - i_{R_4}] = v_{pv} \left[\frac{v_{pv} - v_{es}}{R_3} - \frac{v_{ug} - v_{pv}}{R_4} \right] \quad (14c)$$

$$P_{loads} = v_{loads} i_{loads} = v_{loads} [i_{R_1} - i_{R_2}] = v_{loads} \left[\frac{v_{es} - v_{loads}}{R_1} - \frac{v_{loads} - v_{ug}}{R_2} \right], \quad (14d)$$

where $v_{es}(t)$ and $i_{es}(t)$, $v_{pv}(t)$ and $i_{pv}(t)$, $v_{ug}(t)$ and $i_{ug}(t)$, $v_{loads}(t)$ and $i_{loads}(t)$ denote the voltage and the current on the connecting nodes of the ES, PV, UG and loads system respectively, as in Fig. 1. For the power losses within the DC bus, P_{R_1} , P_{R_2} , P_{R_3} , P_{R_4} , we use the other equivalent power formulation, $P = v^2 \times R$, which allows to deduce the following relations:

$$P_{R_1} = \frac{[v_{es} - v_{loads}]^2}{R_1}, \quad (15)$$

$$P_{R_3} = \frac{[v_{pv} - v_{es}]^2}{R_3}, \quad (16)$$

$$P_{R_2} = \frac{[v_{loads} - v_{ug}]^2}{R_2}, \quad (17)$$

$$P_{R_4} = \frac{[v_{ug} - v_{pv}]^2}{R_4}. \quad (18)$$

The previous relations (14a-18) are important and will be applied later in the construction of the objective function for the power loss minimization problem.

4. Optimization objectives and constraints

At this point, the objectives of the optimization problem and the constraints which need to be taken into account will be detailed.

4.1. Objectives

The main objective of this work is the optimal power flow while minimizing the power dissipation in the DC bus. This problem aims to optimize the power flows within the microgrid such as to minimize the power losses during transmission with the minimum electricity cost. Therefore, the general cost function which penalizes the energy dissipation will be divided in two parts:

- the cost minimization, according to which the electricity cost of the UG power purchase will be penalized. The goal is to sell power to the UG, generated by the renewable resources, and to exploit the ES system towards the consumers' benefit. The cost function which penalizes the electricity cost is written below:

$$J^1(d(t)) = \int_{t_0}^{t_f} e(t) P_{ug} = \int_{t_0}^{t_f} e(t) (P_{loads} + P_{es} - P_{pv}), \quad (19)$$

where reference profiles will be taken into account for the PV and the loads. The P_{ug} is replaced, exploiting the power conservation law ($P_{ug} = P_{loads} + P_{es} - P_{pv}$), without considering the power loss (8);

- the optimal power flow, minimizing the power dissipation in the DC bus. Therefore, the cost function will be the following:

$$J^2(d(t)) = - \int_{t_0}^{t_f} P_R. \quad (20)$$

where $P_R = P_{R_1} + P_{R_2} + P_{R_3} + P_{R_4}$ corresponds to the power loss inside the central network (15-18). Relation (8) is taken into account.

We observe that in both cases the power conservation is taken into account and the control variable is the duty cycle of the switches in the converters, $d(t)$. The ES system and the central transmission network will be analytically included in the optimization problem, utilizing the PH models previously developed here and in [10].

4.2. Constraints

This subsection will describe the general constraints which will be taken into account for the energy management problem. As already mentioned, the ES system is a major component of the overall scheme. The batteries have a limited lifetime which

demands to respect certain constraints concerning the battery's characteristics. Therefore, the constraints for the ES system are (see also Fig. 2):

$$\begin{aligned} q_{1b}^{\min} &\leq q_{1b}(t) \leq q_{1b}^{\max}, \\ q_{2b}^{\min} &\leq q_{2b}(t) \leq q_{2b}^{\max}, \end{aligned}$$

Charging mode :

$$\begin{aligned} v_{b,\text{charging}}^{\min} &\leq v_{b,\text{charging}}(t) \leq v_{b,\text{charging}}^{\max}, \\ i_{b,\text{charging}}^{\min} &\leq i_{b,\text{charging}}(t) \leq i_{b,\text{charging}}^{\max}, \end{aligned}$$

Discharging mode :

$$\begin{aligned} v_{b,\text{discharging}}^{\min} &\leq v_{b,\text{discharging}}(t) \leq v_{b,\text{discharging}}^{\max}, \\ i_{b,\text{discharging}}^{\min} &\leq i_{b,\text{discharging}}(t) \leq i_{b,\text{discharging}}^{\max}. \end{aligned}$$

In addition to these constraints, the output voltage on the connecting nodes in the DC-bus must be always close to a certain voltage value, $v_{DC} = 400$ V in this case. Therefore, according to Fig. 1, the limitations considered for the connecting nodes are given below (taking into account that $v_{DC}^{\min,h}$ and $v_{DC}^{\max,h}$ will set the limits to keep the DC voltage on every connecting node close to the nominal):

$$v_{DC}^{\min,h} \leq v_{ug}(t) \leq v_{DC}^{\max,h}, \quad (21a)$$

$$v_{DC}^{\min,h} \leq v_{pv}(t) \leq v_{DC}^{\max,h}, \quad (21b)$$

$$v_{DC}^{\min,h} \leq v_{es}(t) \leq v_{DC}^{\max,h}, \quad (21c)$$

$$v_{DC}^{\min,h} \leq v_{loads}(t) \leq v_{DC}^{\max,h}. \quad (21d)$$

Furthermore, the duty cycles d_{1sc} and d_{2sc} of the Split-Pi converter are limited into the interval referred below:

$$0 \leq d_{1sc} \leq 1, \quad (22)$$

$$0 \leq d_{2sc} \leq 1. \quad (23)$$

Finally, an upper and a lower limit must be defined also for the external grid power generation as follows:

$$P_{ug}^{\min} \leq P_{ug}(t) \leq P_{ug}^{\max}, \quad (24)$$

with $P_{ug}(t) = v_{ug}(t)i_{ug}(t)$.

4.2.1. Flat representation of the ES connected to the Split-Pi converter

Hereinafter, for the flat representation of the ES dynamical model (1a)-(1g), the flat outputs found in [10] will be recalled:

$$z_1(t) = \frac{1}{I_{1sc}} \frac{p_{1sc}(t)^2}{2} + \frac{1}{I_{2sc}} \frac{p_{2sc}(t)^2}{2} + \frac{1}{C_{2sc}} \frac{q_{2sc}(t)^2}{2}, \quad (25a)$$

$$z_2(t) = q_{3sc}(t) + q_{1b}(t), \quad (25b)$$

$$z_3(t) = q_{2b}(t), \quad (25c)$$

$$z_4(t) = q_{2sc}(t). \quad (25d)$$

Replacing (25a)–(25d) into the PH model (1a-1g), we obtain the flat representation of the system, hence the states and the inputs in function of the flat outputs. Finally, the acquired equations are written in function of the flat outputs.

Since the ES system has been already written in function of the flat outputs, the ES voltage and the current, $v_{es}(t)$ and $i_{es}(t)$, can be written in function of a family of N B-splines functions of order d which are denoted as $b_{i,d}(t)$. These basis functions are

summed together (and weighted through their control points p_i) in order to describe the flat output $z_3(t)$. Hence, writing the flat output z_3 (25c) in function of the B-spline curves, $z_3(t) = \sum_{i=1}^N p_i b_{i,d}(t) = \mathcal{P} \mathcal{B}_d(t)$, we can now express (26a) and (26b) by exploiting the derivation property of B-splines (which allows to characterize derived splines in terms of lower order splines; matrices $M_{d,d-1}$, $S_{\kappa,d-1,d}$ are computed accordingly as may be seen for example in [20]). Through the B-spline derivation property, we parametrize firstly the voltage of the battery, v_b , and the current of the battery, i_b , in function of which the ES voltage and the current, $v_{es}(t)$ and $i_{es}(t)$, are written (5a-5b). Therefore, we have the following:

$$p_i^{v_b} = \frac{1}{C_{2b}} p_i + R_{2b} (\mathcal{P} M_{d,d-1} S_{\kappa,d-1,d})_i, \quad (26a)$$

$$p_i^{i_b} = \left(1 + \frac{C_{1b}}{C_{2b}}\right) (\mathcal{P} M_{d,d-1} S_{\kappa,d-1,d})_i + C_{1b} R_{2b} \cdot (\mathcal{P} M_{d,d-2} S_{\kappa,d-2,d})_i, \quad (26b)$$

where $p_i^{v_b}$ and $p_i^{i_b}$ are the control points for the voltage and the current of the battery respectively. Next, for $v_b(t)$ and $i_b(t)$ as already presented in [10], we have:

$$v_b(t) = \sum_{i=1}^N \left[\frac{1}{C_{2b}} p_i + R_{2b} (\mathcal{P} M_{d,d-1} S_{\kappa,d-1,d})_i \right] b_{i,d}(t), \quad (27a)$$

$$i_b(t) = \sum_{i=1}^N \left[\left(1 + \frac{C_{1b}}{C_{2b}}\right) (\mathcal{P} M_{d,d-1} S_{\kappa,d-1,d})_i + C_{1b} R_{2b} \cdot (\mathcal{P} M_{d,d-2} S_{\kappa,d-2,d})_i \right] \cdot b_{i,d}(t), \quad \forall t \in [\tau_\kappa, \tau_{\kappa+1}). \quad (27b)$$

where N is the number of control points p , r is the derivative of the B-splines, d is the order of the B-spline, $b_{i,d}(t)$ is the i_{th} B-spline of order d , κ is the number of knots and τ_κ is the κ^{th} knot, $\mathcal{B}(t)$ is the vector of the B-splines and \mathcal{P} is the matrix of control points $\in \mathbb{R}^{3 \times N}$. Additionally, $S_{\kappa,d-r,d}$ is the translation matrix from higher to lower degree basis functions and $\mathcal{M}_{d,d-r}$ is the matrix which performs the linear combinations of the lower-degree basis functions.

5. Hierarchical control approach with constrained optimization

This section presents analytically the hierarchical control problem describing the high and the middle level when not ignoring the power losses in the central transmission-line network. The optimal power profiles for the ES, P_{es} , and the UG, P_{ug} , are provided by minimizing the electricity cost and the power dissipation. At the high and the middle level, the whole dynamics of the ES system is taken into account, as it will be shown later, in order to link the power losses of the central transmission network to the battery dynamics. Afterwards, the optimal profiles obtained at the high level are used as references at the middle level for tracking under perturbation, where the control variable is the output voltage of the Split-Pi converter, v_{sc_out} , as in Fig. 2. The discretized model of the battery is considered, already presented in [10], and the main objective is the reduction of the deviations among the reference and the actual values. Finally, at the low level, the tracking profiles of the voltage and the current of the battery, as well as the input voltage of the ES system, v_{es} , are applied to the ES PH model to control the switching activity within the Split-Pi converter.

As aforementioned, the flatness-based optimization approach of [10] is reformulated adding the power losses within the central network as in Fig. 1. Therefore, the dynamics of the system change and the problem becomes more complicated because of the relations among the voltage, the current and the power of the DERs, the consumers' demand and the power losses. In the present case, since the power losses in the central transmission lines are considered, the voltage in the common DC-bus will not be stable and it will vary regarding the constraints of (21). On each connecting node a different voltage value

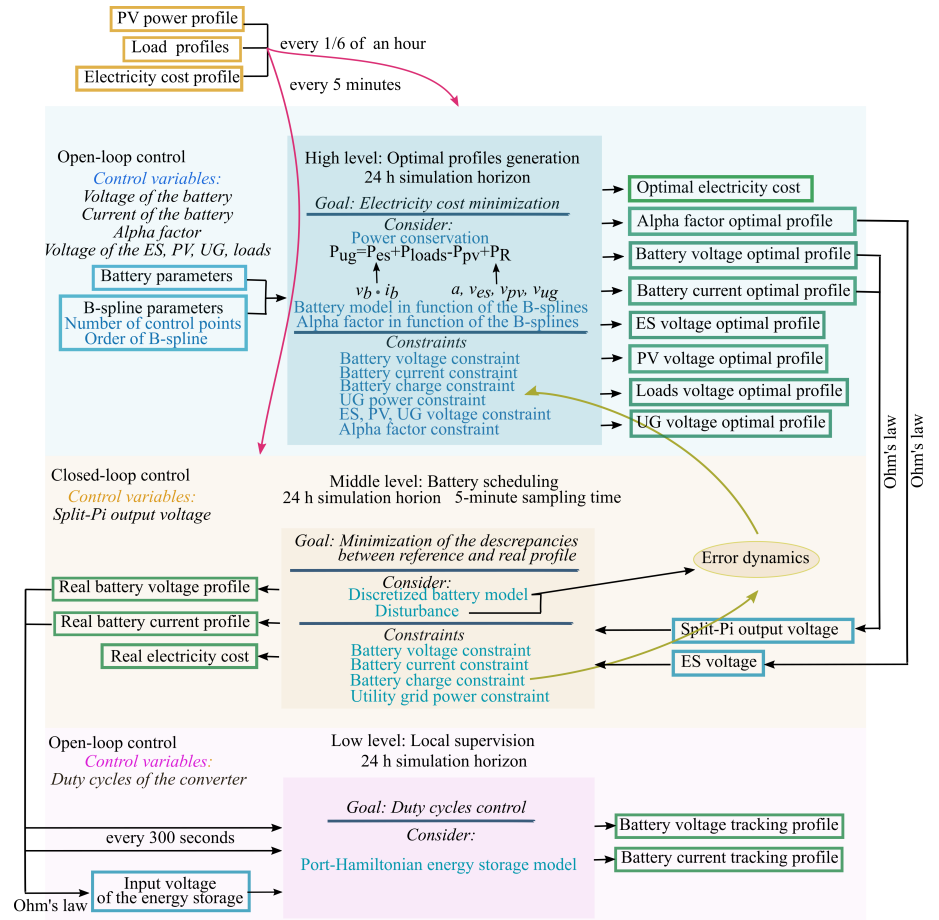


Figure 4. Flowchart of the proposed hierarchical control strategy of the DC microgrid considering the power losses in the central transmission network.

will appear, because of the voltage drop created by the resistors. Therefore, a different notation for the voltage and the current on each connecting node is necessary.

In Fig. 4, the control scheme of the energy management problem, under the presence of power losses in the central transmission network, is illustrated. The control variables are the voltage, v_b , and the current, i_b , of the battery, the voltages on the connecting nodes of the ES, v_{es} , the PV, v_{pv} , the UG, v_{ug} , and the loads, v_{loads} , and the α factor, which defines the relations among the duty cycles, d_{1sc} and d_{2sc} , in the Split-Pi converter. Optimal profiles are generated for the ES system, the duty cycles through the α factor and the voltages on the connecting nodes.

5.1. High level

This section will introduce the optimization problem of the high level including details for its flat representation and B-spline parametrization for continuous-time constraint validation.

5.1.1. Definition of the optimization problem with the power loss included

The principal objective of the high level problem is the generation of reference trajectories in continuous time, exploiting the flat output representation of the ES system. Therefore, an optimal scheduling for the battery charging and discharging is obtained and, in the meantime, the electrical power purchase from the UG is minimized. The general cost function considered at the high level is the following:

$$\mathcal{J} = \int_{t_0}^{t_f} e(t) P_{ug} dt, \quad (28)$$

where $e(t)$ is the electricity price.

At first, the power losses are taken into consideration (8), hence $P_{ug}(t)$ is equal to:

$$\begin{aligned} P_{ug}(t) &= P_{es}(t) + P_{loads}(t) - P_{pv}(t) + P_R(t) \Rightarrow \\ \Rightarrow P_{es}(t) &= P_{ug}(t) - P_{loads}(t) + P_{pv}(t) - P_R(t), \end{aligned} \quad (29a)$$

where $P_R(t) = P_{R1}(t) + P_{R2}(t) + P_{R3}(t) + P_{R4}(t)$ is the total power loss created by the four resistors existing in the central network. Hereinafter, the objective function is analytically calculated and has the following form:

$$\mathcal{J} = \int_{t_0}^{t_f} e(t) (P_{es}(t) + P_{loads}(t) - P_{pv}(t) + P_R(t)) dt \quad (30)$$

and the complete optimization problem becomes:

$$\min_{i_b, v_b, \alpha, v_{es}, v_{pv}, v_{ug}} \int_{t_0}^{t_f} e(t) [\underbrace{P_{es}(t)}_{i_b(t)v_b(t)} + P_{loads}(t) - P_{pv}(t) + P_R(t)] dt, \quad (31a)$$

$$\text{subject to : the system dynamics (1a) – (1g),} \quad (31b)$$

$$\text{the power conservation (29a),} \quad (31c)$$

$$v_{DC}^{min,h} \leq v_{ug}(t), v_{pv}(t), v_{es}(t), v_{loads}(t) \leq v_{DC}^{max,h}, \quad (31d)$$

$$v_b^{min,h} \leq v_b(t) \leq v_b^{max,h}, \quad (31e)$$

$$i_b^{min,h} \leq i_b(t) \leq i_b^{max,h}, \quad (31f)$$

$$q_{2b}^{min,h} \leq q_{2b}(t) \leq q_{2b}^{max,h}, \quad (31g)$$

$$\begin{aligned} P_{ug}^{min,h} - P_{loads}(t) + P_{pv}(t) - P_R(t) &\leq P_{es}(t) \\ P_{es}(t) &\leq P_{ug}^{max,h} + P_{loads}(t) - P_{pv}(t) - P_R(t). \end{aligned} \quad (31h)$$

185 Additionally, the following are also considered to write the final form of the objective function of (31a):

- from (10), the voltage, v_{loads} , on the connecting node 1 is written in function of the input voltage, v_{es} , and the input current, i_{es} , of the ES system:

$$v_{loads}(t) = R_1 i_{es}(t) + (1 + \frac{R_1}{R_3}) v_{es}(t) - \frac{R_1}{R_3} v_{pv}(t); \quad (32)$$

- from (10), the constraint for the consumer's demand is considered as follows:

$$\begin{aligned} P_{loads}(t) - \epsilon_{loads} &\leq v_{loads}(t) \left[\frac{v_{es}(t) - v_{loads}(t)}{R_1} - \frac{v_{loads}(t) - v_{ug}(t)}{R_2} \right] \leq \\ &\leq P_{loads}(t) + \epsilon_{loads}, \end{aligned} \quad (33)$$

where ϵ_{loads} is the soft constraint to relax the load's demand in order to ensure the feasibility of the optimization problem.

The voltages on the connecting nodes, v_{es} , v_{ug} , v_{loads} and v_{pv} , obey to (21). Finally, the $\alpha(t)$ factor and the $P_{ug}(t)$ (taking into account also (29a)) will be:

$$0 < \alpha(t) < 1, \quad (34a)$$

$$P_{ug}^{min,h} \leq P_{ug}(t) \leq P_{ug}^{max,h} \Rightarrow \quad (34b)$$

$$\begin{aligned} \Rightarrow P_{ug}^{min,h} &\leq P_{es}(t) - P_{pv}(t) + P_{loads}(t) + P_{R1}(t) + P_{R2}(t) + P_{R3}(t) + \\ &+ P_{R4}(t) \leq P_{ug}^{max,h}. \end{aligned}$$

5.2. Flat representation and B-spline parametrization of the optimization problem

Next, the optimization problem in (31a)-(31h) is rewritten in function of the flat outputs (25a)-(25d). The cost function is expressed in terms of the relations in (15)-(18). The flat representations of the $v_{es}(t)$ and $i_{es}(t)$ variables of the ES system are deduced in function of the $v_b(t)$ and $i_b(t)$ flat representations as previously presented in [10]. Substituting (15)-(18) in (30), the cost function becomes:

$$\mathcal{J} = \int_{t_0}^{t_f} e(t) \left[Q_{cost} \left(\underbrace{P_{es}(t)}_{v_{es}(t)i_{es}(t)} - P_{pv}(t) + P_{loads}(t) \right) + Q_{loss} \left(\frac{(v_{es}(t) - v_{loads}(t))^2}{R_1} + \frac{(v_{loads}(t) - v_{ug}(t))^2}{R_2} + \frac{(v_{ug}(t) - v_{pv}(t))^2}{R_4} + \frac{(v_{pv}(t) - v_{es}(t))^2}{R_3} \right) \right] dt. \quad (35a)$$

where $v_{es}(t), i_{es}(t), P_{es}(t)$ are defined by (5a), (5b), (6) respectively. Since the variables $v_{es}(t)$ and $i_{es}(t)$ are written in function of the voltage and the current of the battery, v_b and i_b , they can be written also in function of the B-splines according to (27a) and (27b). Similarly, (34a) and (34b) must be also written in function of the B-splines. The α factor is, firstly, parametrized considering $\frac{1}{\alpha(t)} \in (1, +\infty)$ and a set of B-splines basis functions of order d_α as follows:

$$\frac{1}{\alpha(t)} = \sum_{j=1}^{N_\alpha} p_j^\alpha b_{i,d_\alpha}(t) \quad (36)$$

where N_α is the number of control points p_i^α . Then, applying Theorem A1 from H, a sufficient condition for ensuring (31a) is that each of the scalar control points are supraunitary:

$$p_i^\alpha > 1, \forall i = 1, \dots, N_\alpha. \quad (37)$$

Since α lies in the interval of $(0, 1)$, meaning that it is positive, the following can be considered for the second part of (5a):

$$-R_{1sc}|i_b(t)| \leq R_{1sc}\alpha(t)i_b(t) \leq R_{1sc}|i_b(t)|. \quad (38)$$

Therefore, the constraint $v_{DC}^{min,h} \leq v_{es}(t) \leq v_{DC}^{max,h}$, where v_{es} is considered as in (5a), is valid if and only if:

$$\frac{v_b(t) + i_b(t)R_{1b}}{\alpha(t)} - R_{1sc}|i_b(t)| \geq v_{DC}^{min,h}, \quad (39a)$$

$$\frac{v_b(t) + i_b(t)R_{1b}}{\alpha(t)} + R_{1sc}|i_b(t)| \leq v_{DC}^{max,h}. \quad (39b)$$

Then, for (21) and (34b), (5a), (5b) and (6) are combined to arrive to the following:

$$(p_i^{v_b} + R_{1b}p_i^{i_b})p_j^\alpha - R_{1sc}|p_i^{i_b}| \geq v_{DC}^{min,h}, \quad (40a)$$

$$(p_i^{v_b} + R_{1b}p_i^{i_b})p_j^\alpha + R_{1sc}|p_i^{i_b}| \leq v_{DC}^{max,h}, \quad (40b)$$

where $p_{\kappa,i}^{v_b}$ and $p_{\kappa,i}^{i_b}$ are defined by (26a) and (26b) and κ, i and $j \in \mathbb{N}$ satisfy $d - 1 \leq \kappa \leq n - 1$, $\kappa - d + 2 \leq i \leq \kappa + 1$ and $1 \leq j \leq N_\alpha$. After various computations, which is

given explicitly in I, the previous inequalities are replaced by the sufficient formulations:

$$\begin{aligned} v_{DC}^{min,h} &\leq \sum_{i=1}^N \sum_{j=1}^{N_\alpha} (p_i^{v_b} + R_{1b} p_i^{i_b}) p_j^\alpha b_{i,j,d}(t) - \sum_{i=1}^N \sum_{j=1}^{N_\alpha} R_{1sc} |p_i^{i_b}| p_j^\alpha b_{i,j,d}(t) \leq \\ &\leq \sum_{i=1}^N \sum_{j=1}^{N_\alpha} [p_i^{v_b} + R_{1b} p_i^{i_b} - R_{1sc} |p_i^{i_b}|] p_j^\alpha b_{i,j,d}(t), \end{aligned} \quad (41a)$$

$$\begin{aligned} v_{DC}^{max,h} &\geq \sum_{i=1}^N \sum_{j=1}^{N_\alpha} (p_i^{v_b} + R_{1b} p_i^{i_b}) p_j^\alpha b_{i,j,d}(t) + \sum_{i=1}^N \sum_{j=1}^{N_\alpha} R_{1sc} |p_i^{i_b}| p_j^\alpha b_{i,j,d}(t) \geq \\ &\geq \sum_{i=1}^N \sum_{j=1}^{N_\alpha} [(p_i^{v_b} + R_{1b} p_i^{i_b}) + R_{1sc} |p_i^{i_b}|] p_j^\alpha b_{i,j,d}(t). \end{aligned} \quad (41b)$$

Concerning the constraint of the $P_{ug}(t)$, from (12), it is defined below:

$$\begin{aligned} P_{ug}(t) = v_{ug}(t) i_{ug}(t) = v_{ug}(t) [i_{R_4}(t) - i_{R_2}(t)] = v_{ug}(t) \left(\frac{v_{ug}(t) - v_{pv}(t)}{R_4} - \right. \\ \left. - \frac{v_{loads}(t) - v_{ug}(t)}{R_2} \right) = v_{ug}^2(t) \left(\frac{1}{R_4} + \frac{1}{R_2} \right) - v_{ug}(t) \left(\frac{v_{pv}(t)}{R_4} + \frac{v_{loads}(t)}{R_2} \right). \end{aligned} \quad (42)$$

Replacing $v_{loads}(t)$ with (32) leads to:

$$\begin{aligned} P_{ug}(t) = v_{ug}^2(t) \left(\frac{1}{R_4} + \frac{1}{R_2} \right) - \frac{1}{R_4} v_{ug}(t) v_{pv}(t) - v_{ug}(t) [R_1 i_{es}(t) + \\ + \left(1 + \frac{R_1}{R_3} \right) v_{es}(t) - \frac{R_1}{R_3} v_{pv}(t)]. \end{aligned} \quad (43)$$

Including also (5a) and (5b), $P_{ug}(t)$ is denoted as:

$$\begin{aligned} P_{ug}(t) = v_{ug}^2(t) \left(\frac{1}{R_4} + \frac{1}{R_2} \right) + v_{ug}(t) v_{pv}(t) \left(\frac{R_1}{R_2 R_3} - \frac{1}{R_4} \right) - \\ - \frac{1}{R_2} v_{ug}(t) [R_1 \alpha(t) i_b(t) + \left(1 + \frac{R_1}{R_3} \right) \frac{v_b(t) + R_{1b} i_b(t)}{\alpha(t)} + R_{1sc} \alpha(t) i_b(t)] = \\ = v_{ug}^2(t) \left(\frac{1}{R_4} + \frac{1}{R_2} \right) + v_{ug}(t) v_{pv}(t) \left(\frac{R_1}{R_2 R_3} - \frac{1}{R_4} \right) - \\ - \frac{1}{R_2} v_{ug}(t) \left[\left(1 + \frac{R_1}{R_3} \right) \frac{v_b(t) + R_{1b} i_b(t)}{\alpha(t)} + \left(R_1 + R_{1sc} + \frac{R_1 R_{1sc}}{R_3} \right) \alpha(t) i_b(t) \right]. \end{aligned} \quad (44)$$

Therefore, finally, the constraint (34b) is defined as:

$$\begin{aligned} P_{ug}^{max,h} &\geq v_{ug}^2(t) \left(\frac{1}{R_4} + \frac{1}{R_2} \right) + v_{ug}(t) v_{pv}(t) \left(\frac{R_1}{R_2 R_3} - \frac{1}{R_4} \right) \\ &- \frac{1}{R_2} v_{ug}(t) \left[\left(1 + \frac{R_1}{R_3} \right) \frac{v_b(t) + R_{1b} i_b(t)}{\alpha(t)} - \left(R_1 + R_{1sc} + \frac{R_1 R_{1sc}}{R_3} \right) |i_b(t)| \right], \end{aligned} \quad (45a)$$

$$\begin{aligned} P_{ug}^{min,h} &\leq v_{ug}^2(t) \left(\frac{1}{R_4} + \frac{1}{R_2} \right) + v_{ug}(t) v_{pv}(t) \left(\frac{R_1}{R_2 R_3} - \frac{1}{R_4} \right) \\ &- \frac{1}{R_2} v_{ug}(t) \left[\left(1 + \frac{R_1}{R_3} \right) \frac{v_b(t) + R_{1b} i_b(t)}{\alpha(t)} + \left(R_1 + R_{1sc} + \frac{R_1 R_{1sc}}{R_3} \right) |i_b(t)| \right]. \end{aligned} \quad (45b)$$

Additionally, considering that $-|i_b(t)| \leq \alpha(t)i_b(t) \leq |i_b(t)|$ and $\frac{v_b(t) + R_{1b}i_b(t)}{\alpha(t)} > 0$ we can rewrite the two previous constraints, (45a) and (45b), as follows:

$$(1 + \frac{R_1}{R_3}) \frac{v_b(t) + R_{1b}i_b(t)}{\alpha(t)} - (R_1 + R_{1sc} + \frac{R_1 R_{1sc}}{R_3}) |i_b(t)| \geq -\frac{R_2}{v_{ug}(t)} [P_{ug}^{max,h} - v_{ug}^2(t)(\frac{1}{R_4} + \frac{1}{R_2}) - v_{ug}(t)v_{pv}(t)(\frac{R_1}{R_2 R_3} - \frac{1}{R_4})], \quad (46a)$$

$$(1 + \frac{R_1}{R_3}) \frac{v_b(t) + R_{1b}i_b(t)}{\alpha(t)} + (R_1 + R_{1sc} + \frac{R_1 R_{1sc}}{R_3}) |i_b(t)| \leq -\frac{R_2}{v_{ug}(t)} [P_{ug}^{min,h} - v_{ug}^2(t)(\frac{1}{R_4} + \frac{1}{R_2}) - v_{ug}(t)v_{pv}(t)(\frac{R_1}{R_2 R_3} - \frac{1}{R_4})]. \quad (46b)$$

Next, through (A54a) and (A54b) in I, the left part of (46a) and (46b) is defined in function of the B-splines:

$$(1 + \frac{R_1}{R_3}) \frac{v_b(t) + R_{1b}i_b(t)}{\alpha(t)} \pm (R_1 + R_{1sc} + \frac{R_1 R_{1sc}}{R_3}) |i_b(t)| = (1 + \frac{R_1}{R_3}) \cdot \sum_{i=1}^N \sum_{j=1}^{N_\alpha} (p_i^{v_b} + R_{1b}p_i^{i_b}) p_j^\alpha b_{i,j,d}(t) \pm (R_1 + R_{1sc} + \frac{R_1 R_{1sc}}{R_3}) \sum_{i=1}^N \sum_{j=1}^{N_\alpha} |p_i^{i_b}| b_{i,j,d}(t), \quad (47)$$

190 which is proven similarly as in (A55a) and (A55b).

Hence, the optimization problem of (31a)-(31h) becomes:

$$\min_{p, p^\alpha, v_{pv}(t), v_{ug}(t)} \int_{t_0}^{t_f} e(t) \left[Q_{cost} [(v_b(t) + i_b(t)R_{1b})i_b(t) + R_{1sc}(\alpha(t)i_b(t))^2 - P_{pv}(t) + \right. \quad (48a)$$

$$\left. + P_{loads}(t)] + Q_{loss} \left[-\frac{(v_b(t) + i_b(t)R_{1b})}{\alpha(t)} + R_{1sc}\alpha(t)i_b(t) - v_{loads}(t))^2}{R_1} + \right. \quad (48b)$$

$$\left. + \frac{(v_{loads}(t) - v_{ug}(t))^2}{R_2} + \frac{(v_{pv}(t) - \frac{v_b(t) + i_b(t)R_{1b}}{\alpha(t)} + R_{1sc}\alpha(t)i_b(t))^2}{R_3} + \right. \quad (48c)$$

$$\left. + \frac{(v_{ug}(t) - v_{pv}(t))^2}{R_4} \right] dt \quad (48d)$$

$$\text{subject to : the system dynamics (1a) - (1g),} \quad (48e)$$

$$\text{the power conservation (29a),} \quad (48f)$$

$$\text{the voltage constraints on the connecting nodes (21)} \quad (48g)$$

$$v_b^{min,h} \leq \sum_{i=1}^N p_i^{v_b} b_{i,d}(t) \leq v_b^{max,h}, \quad (48h)$$

$$i_b^{min,h} \leq \sum_{i=1}^N p_i^{i_b} b_{i,d}(t) \leq i_b^{max,h}, \quad (48i)$$

$$q_{2b}^{min,h} \leq \sum_{i=1}^N p_i b_{i,d}(t) \leq q_{2b}^{max,h}, \quad (48j)$$

$$\text{the } P_{ug} \text{ constraints (45a), (45b),} \quad (48k)$$

$$\text{the central network relations constraints (32), (33),} \quad (48l)$$

where $v_b(t)$ and $i_b(t)$ are written in terms of the B-splines as in (27a) and (27b) respectively. Q_{cost} and Q_{loss} are the weight matrices corresponding to the cost minimization and power loss mitigation.

5.3. Middle level

195 The middle level of the hierarchical problem is analyzed next. Note that the reference profiles obtained at the high level for the battery current, i_b , battery voltage, v_b , and input voltage of the ES system v_{es} will be denoted here as i_b^{ref} , v_b^{ref} and v_{es}^{ref} , respectively. Similarly for the α factor which is also mentioned at the middle level as α^{ref} .

Hence, a tube-MPC controller is introduced to track the output voltage reference profile, $v_{sc_out}^{ref}$, of the Split-Pi converter under perturbation. Consider that the output voltage reference of the converter can be written in function of the battery current and voltage reference profiles obtained at the high level (4b):

$$v_{sc_out}^{ref}(t) = v_b^{ref}(t) + i_b^{ref}(t)R_{1b}, \quad (49)$$

200 according to Ohm's law obtained from the electrical circuit (Fig. 2). At this level, the battery's dynamics will be discretized through the standard Euler discretization as presented in [10].

At this point, we continue using the tube-MPC controller and the discretized dynamics of the system. However, since the power losses are taken into account, the MPC tracking problem is reformulated as follows:

$$\min_{\tilde{u}(k)} \sum_{i=k}^{k+N_p-1} (\tilde{v}_{es}(i) - \tilde{v}_{es}^{ref}(i))^T Q_{\tilde{v}_{es}} (\tilde{v}_{es}(i) - \tilde{v}_{es}^{ref}(i)) + (\tilde{u}(i) - \tilde{u}^{ref}(i))^T R_{\tilde{u}} (\tilde{u}(i) - \tilde{u}^{ref}(i)) \quad (50a)$$

$$\text{subject to : the system discretized dynamics,} \quad (50b)$$

$$\tilde{v}_b^{min,m} \leq \tilde{v}_b(k) \leq \tilde{v}_b^{max,m}, \quad (50c)$$

$$\tilde{i}_b^{min,m} \leq \tilde{i}_b(k) \leq \tilde{i}_b^{max,m}, \quad (50d)$$

$$\tilde{q}_{2b}^{min,m} \leq \tilde{q}_{2b}(k) \leq \tilde{q}_{2b}^{max,m}, \quad (50e)$$

$$\tilde{v}_{es}^{min,m} \leq \tilde{v}_{es}(k) \leq \tilde{v}_{es}^{max,m}, \quad (50f)$$

$$\tilde{P}_{ug}^{min,m} \leq \tilde{P}_{ug}(k) \leq \tilde{P}_{ug}^{max,m}. \quad (50g)$$

In the last constraint, $P_{ug}(t)$, the power losses must be considered in the power conservation equation as in (29a) in section 5.1. Therefore, (50g) is replaced by:

$$\tilde{P}_{ug}^{min,m} - \tilde{P}_{loads}(k) + \tilde{P}_{pv}(k) - \tilde{P}_{R_1}(k) - \tilde{P}_{R_2}(k) - \tilde{P}_{R_3}(k) - \tilde{P}_{R_4}(k) \leq \tilde{P}_{es}(k), \quad (51a)$$

$$\tilde{P}_{ug}^{max,m} - \tilde{P}_{loads}(k) + \tilde{P}_{pv}(k) - \tilde{P}_{R_1}(k) - \tilde{P}_{R_2}(k) - \tilde{P}_{R_3}(k) - \tilde{P}_{R_4}(k) \geq \tilde{P}_{es}(k), \quad (51b)$$

where $\tilde{P}_{es}(k) = \tilde{i}_{es}(k)\tilde{v}_{es}(k)$. $\tilde{i}_{es}(k)$ and $\tilde{v}_{es}(k)$ are calculated with respect to the α^{ref} obtained at the high level as in (5a) and (5b):

$$v_{es}(k) = \frac{v_b(k) + i_b(k)R_{1b}}{\alpha^{ref,h}(k)} + R_{1sc}\alpha^{ref}(k), \quad (52a)$$

$$i_{es}(k) = \alpha^{ref}(k)i_b(k). \quad (52b)$$

205 At this point, we mention that the low level remains the same as in [10] since it is a local controller concerning the operation of the Split-Pi converter locally and its dynamics are not influenced by the addition of power losses in the transmission network. The single difference is the input voltage, v_{es} , of the ES system on the connecting node 2, which varies among the considered constraints (21). The tracking profiles obtained for the voltage, v_{es} , at the middle level are considered.

5.4. Low level

In this work, where the power losses are considered, the same process is followed at the low level since it concerns only the ES system. The operation of the Split-Pi converter has been considered defining its switching activity. Here, the duty cycles of the switches are the control variables of the system and the tracking profiles obtained at the middle level are used as references.

For the description of the Split-Pi converter, we follow the patent of United States Patent and Trademark Office No: US 6914420 B2 published on July 2005 [19] as already described in [10]. The patent provides the relations among the input and output voltage, v_{sc_in} and v_{sc_out} , and the duty cycles, d_{1sc} and d_{2sc} , of the converter. Therefore, according to the functioning of the Split-Pi converter, we conclude to the following relation:

$$d_{2sc}(t) = 1 - \frac{v_{es}(t) - \sqrt{v_{es}^2(t) - 4(v_{sc_out}(t) - v_b(t))(v_{sc_out}(t))}}{2(v_{sc_out}(t) - v_b(t))}, \quad (53)$$

which can be valid only if $v_{sc_out}(t) \neq v_b(t)$.

In the case of the transmission network with power loss existence, the same procedure is followed at the low level since it concerns the internal supervision of the ES system.

6. Simulation results

This section presents the simulation results of the three control levels. Table 1 depicts the parameters of the DC microgrid used for the simulations and Table 2 illustrates the variables and constraints for the high and the middle level. To proceed, reference profiles for the PV and the loads are taken into account, based on real irradiation and temperature data. Furthermore, a collection of AGM 12-165 lead acid batteries is considered (165 Ah battery capacity) for the ES system. The DC microgrid is connected to the UG (4200 W maximum UG generation) through a DC breaker. For the simulations we use MATLAB 2015a. Furthermore, YALMIP optimization toolbox [21] was chosen for both high and middle level which allows the use of the IPOPT solver [22] capable to handle nonlinear optimization problems. For the low level, the PH ES system was designed in MATLAB/Simulink in order to validate the proper operation of the switching activity within the Split-Pi converter n[10].

Table 1: Values of the parameters.

Variable	Values	Units
R_{1sc}, R_{1b}, R_{2b}	1, 0.025, 0.088	$[\Omega]$
I_{1sc}, I_{2sc}	0.25, 0.25	$[H]$
$C_{1sc}, C_{2sc}, C_{3sc}$	0.0008, 0.0008, 0.0008	$[F]$
C_{1b}, C_{2b}	86400, 21600	$[F]$
R_1, R_2, R_3, R_4	1	$[\Omega]$

6.1. Simulation results of the high level

In this section, the simulation results of the high level are introduced according to (48a)-(48l). The profiles generated at the high level for the commercial use (CU) (Fig. 5a), where the load is high during the day, and the domestic use (DU) (Fig. 5b), where the load is high during the afternoon, are illustrated. Moreover, the constraints of the system are considered according to the RPI set found in [10].

Concerning the simulations, in the CU case for the *Power Balancing* profiles (Fig. 5a) the consuming hours are during the day. The UG is unable to charge completely the batteries during the night, when the electricity cost is lower, because of the power loss

Table 2: Variables and constraints for the high level.

	Variable	Values	Units
High level	N as in (41a) (41b), (47)	27	
	N_a as in (41a) (41b), (47)	18	
	d_a as in (36)	4	
Constraints	$v_b^{min,h} \leq v_b \leq v_b^{max,h}$	$12 \leq v_b \leq 13$	[V]
	$i_b^{min,h} \leq i_b \leq i_b^{max,h}$	$-9 \leq i_b \leq 9$	[A]
	$q_{1b}^{min,m} \leq q_{1b} \leq q_{1b}^{max,m}$	$288.3 \leq q_{1b} \leq 307.7$	[Ah]
	$q_{2b}^{min,h} \leq q_{2b} \leq q_{2b}^{max,h}$	$72.5 \leq q_{2b} \leq 77.5$	[Ah]
	$P_{ug}^{min,h} \leq P_{ug} \leq P_{ug}^{max,h}$	$-2100 \leq P_{ug} \leq 4200$	[W]
	$v_{DC}^{min,h} \leq v_{ug,pv,es,loads} \leq v_{DC}^{max,h}$	$380 \leq v_{ug,pv,es,loads} \leq 430$	[V]
Middle level	N_p as in (50a)	5	[h]
	$Q_{\tilde{v}_{es}}$ as in (50a)	$diag(1, 1)$	
	$R_{\tilde{u}}$ as in (50a)	800	
Constraints	$v_b^{min,m} \leq \tilde{v}_b \leq v_b^{max,m}$	$11.9 \leq \tilde{v}_b \leq 13.1$	[V]
	$i_b^{min,m} \leq \tilde{i}_b \leq i_b^{max,m}$	$-10.6 \leq \tilde{i}_b \leq 10.6$	[A]
	$q_{1b}^{min,m} \leq \tilde{q}_{1b}(k) \leq q_{1b}^{max,m}$	$287.6 \leq \tilde{q}_{1b}(k) \leq 308.4$	[Ah]
	$q_{2b}^{min,m} \leq \tilde{q}_{2b} \leq q_{2b}^{max,m}$	$72.3 \leq \tilde{q}_{2b} \leq 77.7$	[Ah]
	$P_{ug}^{min,m} \leq \tilde{P}_{ug} \leq P_{ug}^{max,m}$	$-2100 \leq \tilde{P}_{ug} \leq 4200$	[W]
	$v_{DC}^{min,h} \leq v_{ug,pv,es,loads} \leq v_{DC}^{max,h}$	$370 \leq v_{ug,pv,es,loads} \leq 430$	[V]

existing in the transmission lines (only 0.8% for battery charging). After, during the day, UG and PV sources collaborate (in total 99% power production) to satisfy the consumers' demand (97% consumed from the total power). This is possible considering that we keep same resistor values in the transmission lines, $R = 1 \Omega$. In the case where the batteries are closer to the renewable sources, the losses among them are lower and the batteries could be more effectively charged. Also, when the distance among the external grid and the microgrid is higher (meaning higher power loss), then the controller gives priority to the parts which are less affected by the power losses. On the other hand, in DU case where there is no high demand from 12p.m. to 12a.m., the UG and the PV charge the batteries. The consumers' demand increases during the afternoon, while during the day until 3p.m. remains more or less stable. As aforementioned, there is, also, enough energy to sell to the UG (approximately 13% of the total power consumed). Hence, to make profit in a commercial environment, the use of larger installations for the renewable resources is important.

Likewise, the batteries' reference profiles for the current, voltage, state of charge are introduced where the constraints are verified. The electricity cost is also calculated which is 4.318 euros for the CU and 2.713 euros for the DU. The cost without using the ES system is equal to 4.737 euros for the CU profile and 4.732 euros for the DU profile, where we observe that in the first case (CU profile) remains the same since the ES system usage is almost negligible. Although, in the case of the DU profile, the cost without the battery existence is a lot higher, since its usage is exploited in the best possible way.

Afterwards, the power losses are depicted in Fig. 6 together with the constraint validation for the voltage on the four different nodes where the sources and the loads' systems stand. In the CU profile (Fig. 6a), the power losses are higher mostly because of the UG power purchase towards the loads during the day (transmission line R_2 : 0.24% of the total power loss), while in the DU is less (Fig. 6b). Furthermore, we observe that the power losses in lines R_3 and R_4 are similar for both cases because of the PV purchase

towards the UG or the ES system. For transmission line R_1 , with the CU profile, the loss is around 0.12% of the total loss and higher than the DU case since a large amount of power is transmitted from the UG to the loads during the day. While, for the DU, the total loss of R_1 and R_2 , about 0.33%, mostly exists due to the fact that the load demand increases during the afternoon. It is visible from Table 3 that, finally, the power loss is higher in the CU scenario since also the total power produced is higher than in the case of the DU load profile. The calculation time of the simulation is 12 min for the DU load and 6 min for the CU load.

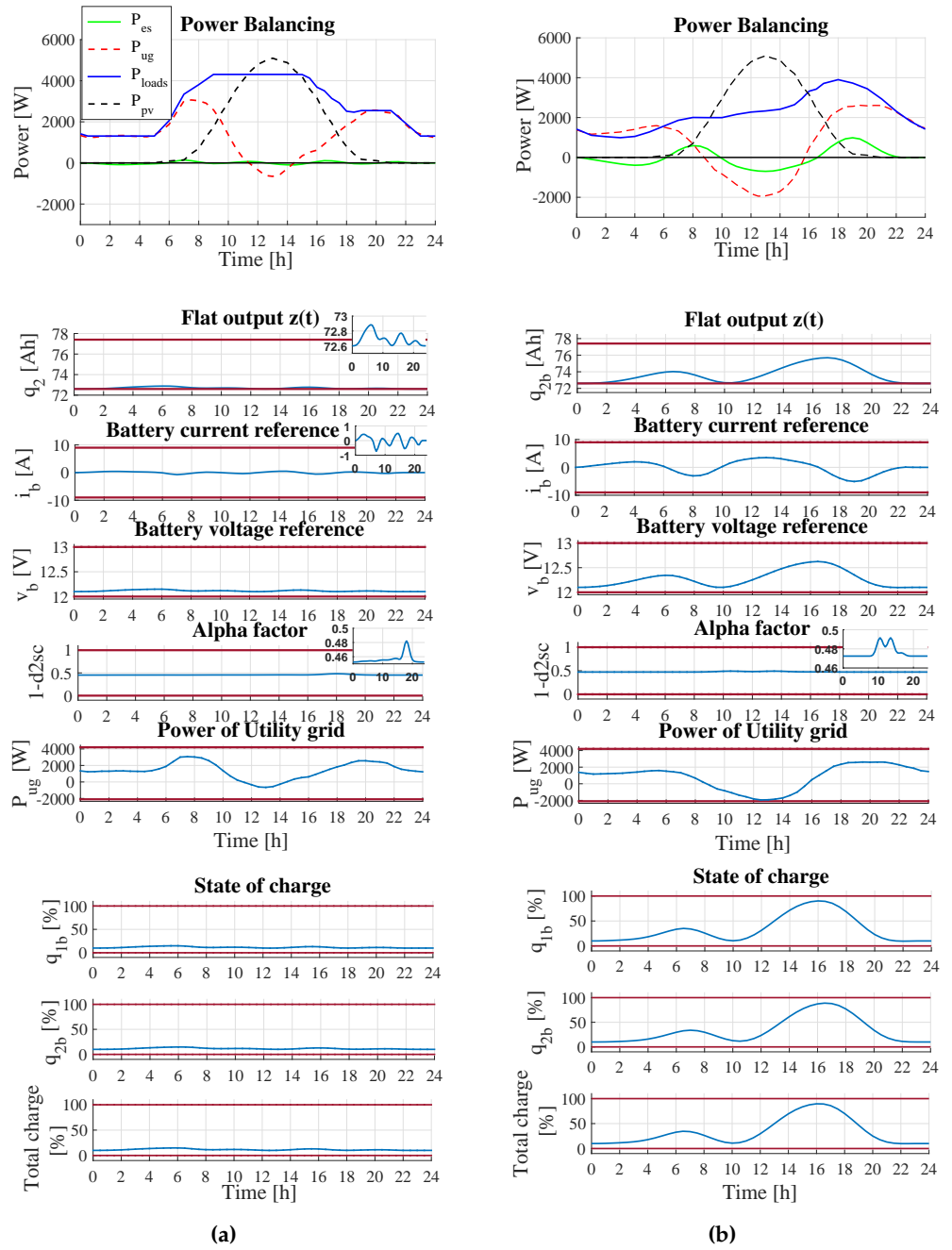


Figure 5. (a) Power balancing, optimal reference profiles and state of charge of the ES system of the CU profile. (b) Power balancing, optimal reference profiles and state of charge of the ES system of the DU profile. The red lines at the upper and lower part represent the corresponding constraints.

Table 3: Percentage of power in respect to the total power produced or consumed.

Load profile	Power	Power produced [%]	Power consumed [%]	Electricity cost [euros]
Commercial	P_{ug}	49.91%	1.78% sold to the UG	4.318
	P_{es}	0.79%	0.76% for ES charging	-
	P_{pv}	49.30%	-	-
	P_{loads}	-	96.9% for load usage	-
	P_{loss}	-	Total: 0.56% R_1 : 0.12% R_2 : 0.24% R_3 : 0.11% R_4 : 0.09%	-
Domestic	P_{ug}	42.14%	13% sold to the UG	2.713
	P_{es}	6.58%	6.7% for ES charging	-
	P_{pv}	51.28%	-	-
	P_{loads}	-	79.66% for load usage	-
	P_{loss}	-	Total: 0.64% R_1 : 0.12% R_2 : 0.21% R_3 : 0.13% R_4 : 0.18%	-

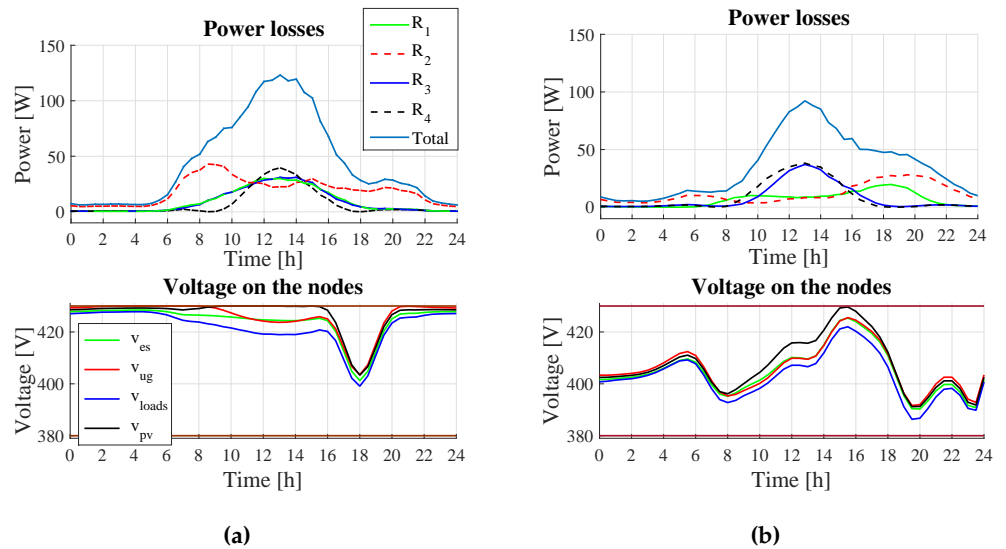


Figure 6. (a) Power losses and voltage on the transmission network nodes for CU profile. (b) Power losses and voltage on the transmission network nodes for DU profile. The red lines at the upper and lower part represent the corresponding constraints.

275 The previous simulations correspond to the expected results. Since, the CU is high during the day, considering also the power losses existing in the transmission line network, the UG is unable to charge the batteries, since it must generate power for the

consumers in cooperation with the PV source. In the DU case, since the consumers' demand is low during the day, similar results are expected as before without including the power losses in the central transmission network. The PV power is able to charge the batteries and sell power to the UG. However, because of the power losses, the power weakens while passing through the transmission lines.

6.2. Simulation results of the middle and low level

This section introduces the results of the middle level using as reference the optimal profiles generated at the high level for the battery current, i_b , and the voltage, v_b as in Fig. 5. Firstly, according to Table 2, the parameters are set for the middle level simulations. As previously mentioned, in the middle level, we use MPC for reference tracking with a prediction horizon N_p equal to 5 and a sampling time T_s equal to 5 min. The system, at

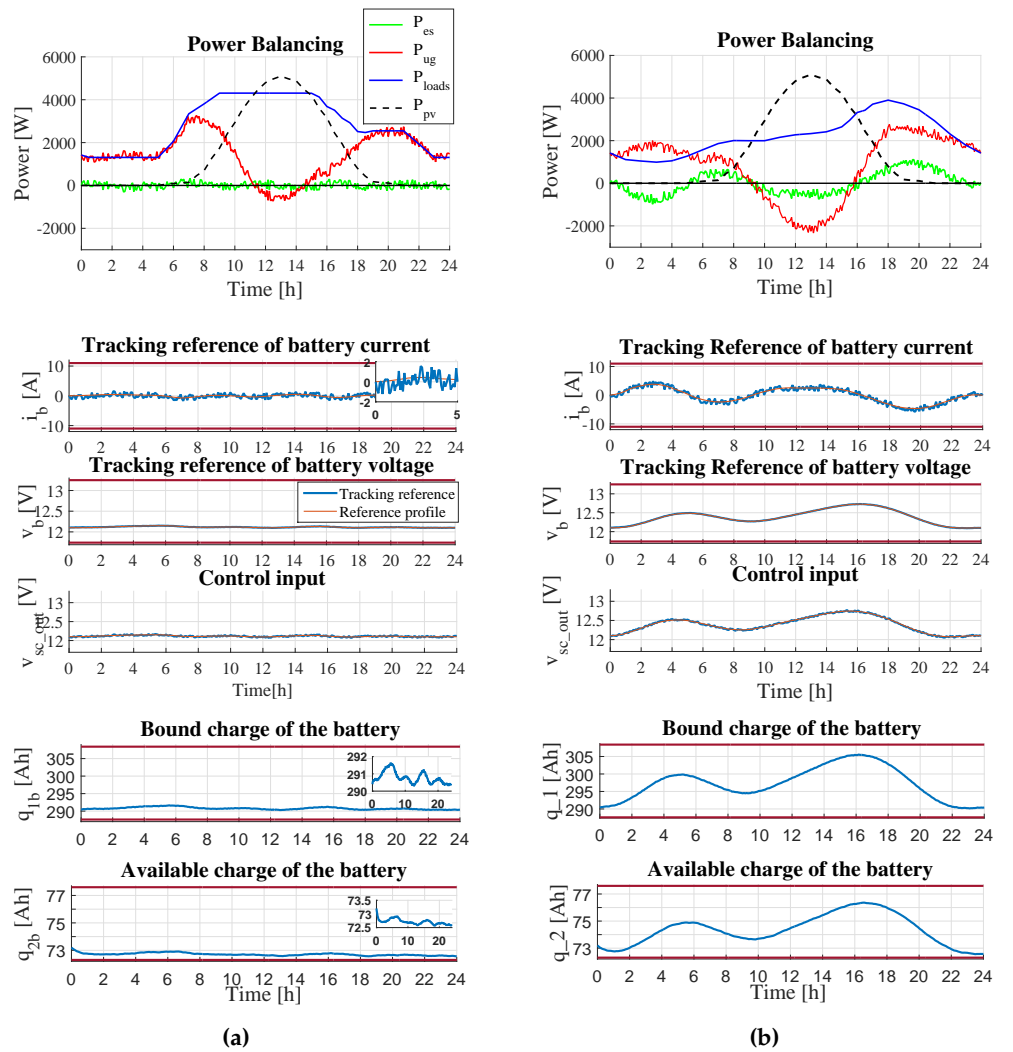


Figure 7. (a) Power balancing, tracking references, available charge and UG power of the commercial load profile. (b) Power balancing, tracking references, available charge and UG power of the domestic load profile. The red lines represent the corresponding constraints.

this point, is discretized and it follows the optimization problem under constraints as in (50a)-(50g) with losses in the transmission network. Additionally, a perturbation is added to the system that is always lower than the difference between the maximum and minimum state value defined by the RPI set in [10].

Table 4: Percentage of power in respect to the total power produced or consumed.

Load profile	Power	Power produced [%]	Power consumed [%]	Power production difference from high level [%]	Power consumption difference from high level [%]
CU	P_{ug}	49.24%	1.85% sold to the UG	-0.62%	0.07%
	P_{es}	2.08%	1.84% for ES charging	1.29%	1.05%
	P_{pv}	48.68%	-	-0.62%	-
	P_{loads}	-	94.74% for load usage	-	0.75%
	P_{loss}	-	1.57%	-	1.01%
DU	P_{ug}	41.27%	13.15% sold to the UG	-0.87%	0.08%
	P_{es}	7.95%	7.73% for ES charging	1.37%	0.97%
	P_{pv}	50.78%	-	-0.5%	-
	P_{loads}	-	77.71% for load usage	-	-1.05%
	P_{loss}	-	1.41%	-	0.77%

In 7, we observe the tracking profiles of the *Power Balancing*, and the control input, v_{sc_out} (the output voltage of the Split-Pi converter), which is in function of the current, i_b , and the voltage, v_b of the battery as in (49). From the figures and the Table 4, where the power produced and the power consumed are illustrated in respect to the total power, we observe that the optimal profiles obtained at the high level are very closely followed.

Furthermore, there are small dissimilarities (less than 1%) between the UG power production/consumption reference and the real profiles as well as the battery's charging/discharging. The cost shortly changes, from 2.713 to 2.708 *euros* for the DU demand and from 4.318 to 4.308 *euros*. The electricity cost decreases slightly, approximately 0.2%, since the UG power production decreases and, in parallel, the power sold to the UG increases. Furthermore, the power loss is higher by 1% for the real profiles because of the slight raise of power generated and transmitted from and to the ES system. Although, in general the errors are low and the reference profiles are well followed. The simulations time endure around 14 *min* for the CU demand and 9 *min* for the DU demand.

In the following, we present the results obtained for the low level following the tracking profiles of the middle level for the battery current, i_b , and the voltage, v_b , under perturbation from Fig. 7. The current, i_b , and the voltage, v_b , of the battery are considered as the reference profiles to follow, taking into account the control law developed in [10]. Apart from the voltage and current reference profiles of the battery, the reference profile of the voltage, v_{es} , entering from the central transmission network is also considered (see Fig. 6a and Fig. 6b).

6.3. Optimal profile generation of different scenarios

Scenario 1: (Different values on the central lines resistors) In here, we consider two different scenarios as in Table 5:

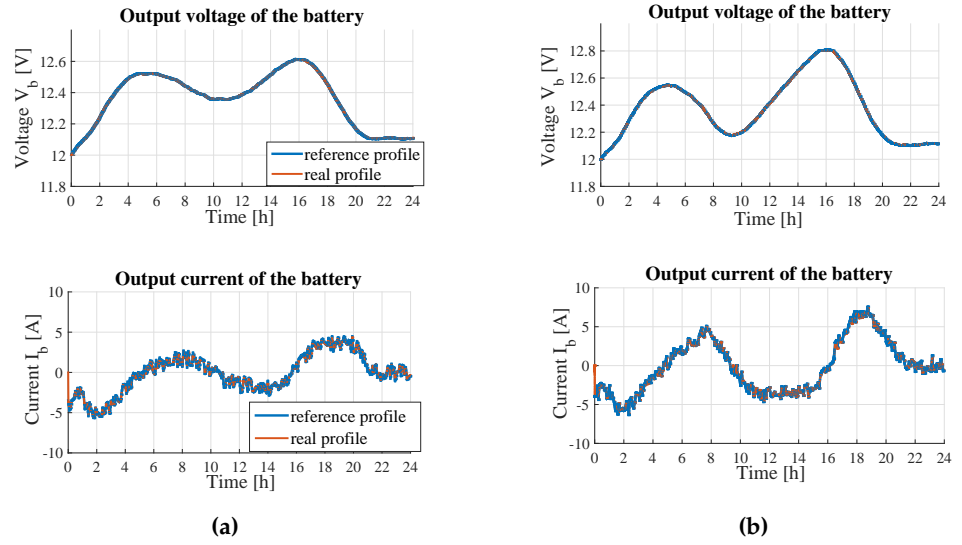


Figure 8. (a) Voltage and current tracking profiles for CU. (b) Voltage and current tracking profiles for DU. (Transmission-line network without power losses)

- for the CU profile, the transmission lines R_1 and R_4 are with different values lower than the R_2 and R_3 considering a greater distance between the UG and the consumers, the PV and the ES than in the previous case;
- for the DU profile, the transmission lines R_1 and R_4 are equal to $1\ \Omega$ (as in section 6.1) and R_2 and R_3 are equal to $3\ \Omega$ keeping this way the renewable resource closer to the UG and the ES closer to the loads.

Table 5: Resistor values for Scenario 2.

Load	Resistors	Value	Unit
Commercial	R_1	0.5	$[\Omega]$
	R_2	5	$[\Omega]$
	R_3	5	$[\Omega]$
	R_4	0.2	$[\Omega]$
Domestic	R_1, R_4	1	$[\Omega]$
	R_2, R_3	3	$[\Omega]$

In the first case, the electricity cost increases for about 30 *cents* compared to the results obtained in section 6.1 for the CU profile, since the power loss among the loads and the UG is higher and, as a result, the external grid generates more power to satisfy the consumers' demand. Furthermore, the PV gives priority to the battery. Since the power loss is less from the battery to the loads, the battery discharges and transmit power towards the consumers. Equal behavior is observed also for the second scenario, where similarly the external grid needs to generate more power because of the loss that exists in R_2 , while the profile of the ES power remains almost the same as in Fig. 5b. Therefore, from the aforementioned results, the number of PVs and batteries close to the load play an important role for the consumers' profit. The power generated from the renewable resources and the batteries must be able to overcome the power losses caused by the UG, reducing this way the UG power generation towards the microgrid.

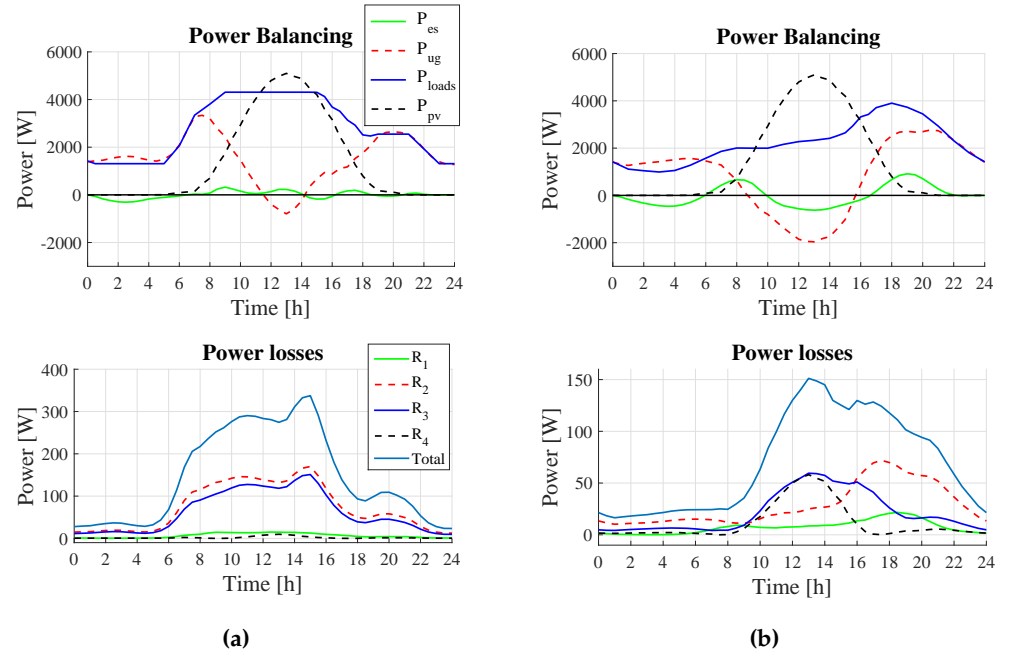


Figure 9. (a) Power balancing and power losses profiles for DU load demand. (b) Power balancing and power losses profiles for CU load demand.

Table 6: Simulation results obtained of Scenario 3.

Load	Power	Power produced [%]	Power consumed [%]	Electricity cost [euros]
CU	P_{ug}	51.2%	1.9% sold to the UG	4.623
	P_{es}	1.9%	2% for ES charging	-
	P_{loads}	-	92% for load usage	-
	P_{pv}	46.9%	-	-
	P_{loss}	-	Total: 4.1% R_1 : 0.19%, R_2 : 2.1%, R_3 : 1.76%, R_4 : 0.05%	-
DU	P_{ug}	44%	13.1% sold to the UG	2.857
	P_{es}	6%	6.7% for ES charging	-
	P_{loads}	-	78.1% for load usage	-
	P_{pv}	50%	-	-
	P_{loss}	-	Total: 2.1% R_1 : 0.2%, R_2 : 0.9%, R_3 : 0.6%, R_4 : 0.4%	-

335 *Scenario 2: (Faulted lines in the transmission network)* In here, considering the DU profile, optimal profiles are generated in case of faulted line events. We consider two scenarios with one faulted line each:

- $R_2 = 0$, the transmission line among the loads and the UG;
- $R_4 = 0$, the transmission line between the PV and the UG system.

340 In the first case, where the transmission line among the loads and the external grid doesn't work, the loss caused by the rest functional lines is higher than in the case of Fig. 5b. The UG generated power is distributed through three lines, hence the loss increases as does the electricity cost. Similar situation is observed in the case of line

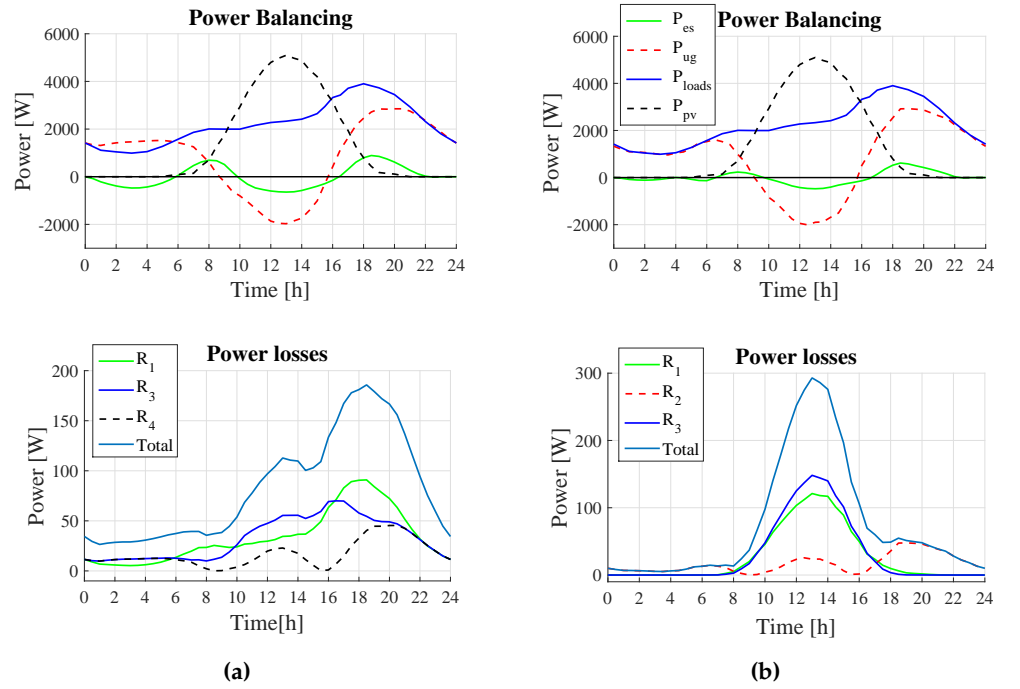


Figure 10. (a) Power balancing and power losses profile generation with R_2 equal to 0. (b) Power balancing and power losses profile generation with R_4 equal to 0.

under fault between the PV and the UG system. The power loss is higher towards the UG system from the PV for selling power than in the case of Fig. 5b. This is because of the interruption of the direct connection among the UG and the PV and, as a result, the power passes through the remaining lines. In general, we observe in both cases, that, finally, the demand is fully satisfied. Therefore, the results validate the meshed topology of the network. In case of a line under fault, the optimization-based controller can meet the consumers' demand through the remaining transmission lines.

Table 7: Simulation results obtained of Scenario 3.

Load	Power	Power produced [%]	Power consumed [%]	Electricity cost [euros]
$R_2=0$	P_{ug}	43%	13.1% sold to the UG	2.881
	P_{es}	6.8%	6.8% for ES charging	-
	P_{loads}	-	77.5% for load usage	-
	P_{pv}	50.2%	-	-
	P_{loss}	-	Total: 2.6% R_1 : 1.09%, R_2 : 0%, R_3 : 0.98%, R_4 : 0.53%	-
$R_4=0$	P_{ug}	43.7%	13.6% sold to the UG	2.765
	P_{es}	3.7%	3.7% for ES charging	-
	P_{loads}	-	80% for load usage	-
	P_{pv}	52.6%	-	-
	P_{loss}	-	Total: 2.7% R_1 : 0.98%, R_2 : 0.61%, R_3 : 1.11%, R_4 : 0%	-

7. Conclusions

The goal of this paper was to extend the hierarchical control problem for a meshed DC microgrid already presented in [10] by adding the power losses in the central transmission network. The main objectives were to develop an optimization problem capable to ensure power balancing in the central transmission network while simultaneously minimizing the power dissipation and the electricity cost. Therefore, high importance was given to the ES system and the central transmission-line network. A constrained optimization-based control strategy applying differential flatness, B-spline parametrization and Model Predictive Control methods was introduced.

The mathematical model of the proposed meshed DC microgrid (Fig.1) composed by a renewable source (PV), an ES system, a collection of DC loads (e.g. EVs, LED lighting, printers, computers and the like) and DC/DC converters was obtained in [14]. The DC microgrid was analyzed interpreting all its components, firstly, as electrical circuits. Each component was studied separately, deriving its mathematical model from the associated Bond graph [16,18]. From the Bond graphs, the PH state-space representation [23] of every element was presented in [14]. Next, in this work, the PH dynamical model of the overall central transmission network was provided replacing the transmission lines by resistors.

Then, the hierarchical control approach was analyzed, divided into three levels, the high, the middle and the low level. An optimization-based approach under constraints was proposed at the high level under the combination of differential flatness and B-spline parametrizations for the PH model. Afterwards, at the middle level, a tracking MPC was developed to follow the optimal profiles obtained at the high level. Finally, the tracking profiles were used at the low level for the local supervision of the ES system.

Since a modeling and an optimization approach were developed for the central transmission network, the operation of the system in case of unexpected events or power outages could be further studied. With the mathematical model developed for the central transmission network, fault mitigation is possible, improving the performance and the reliability of the system.

The reconfiguration of the system may be accomplished at the high level. The optimization problem developed including the power losses in the central transmission network could be used to predict the behavior of the system in case of unexpected events. Generating profiles in case of a line under fault, the corresponding line can be isolated by forecasting the new behavior of the remaining transmission lines. In such a way, the operation of the system continues taking into account the updated optimal profiles. Furthermore, these tools will help in storage sizing for functioning in islanded mode.

Appendix H B-splines properties

The following theorem is considered for the B-spline parametrization of the α factor in (34a).

Theorem A1. [24]: Given scalars $\underline{z}, \bar{z} \in \mathbb{R}$ and a B-spline curve define by $z(t) = \sum_{i=1}^n \mathbf{p}_i \mathbf{b}_{i,d}(t)$ and a knot vector T , a sufficient condition for the validation of

$$\underline{z} \leq z(t) \leq \bar{z}$$

for any $t \in [\tau_\kappa, \tau_{\kappa+1}] \in T$ is that:

$$\underline{z} \leq p_i \leq \bar{z}, \quad \kappa - d + 1 \leq i \leq \kappa$$

390 Appendix I Supplementary calculation for the B-splines

For the constraints (39a,39b), we give explicitly the calculations for their B-spline parametrization. From (27a), (27b), (36) and the B-splines properties [24], we continue as follows (Consider that $\mathbf{b}_{i,j,d}(t) = \mathbf{b}_{i,d}(t)\mathbf{b}_{j,d}(t)$ where $1 \leq i$ and $j \leq n$ and $d = d_\alpha$):

$$\begin{aligned} \frac{v_b(t) + i_b(t)R_{1b}}{\alpha(t)} &= \left[\sum_{i=1}^n \mathbf{p}_{k,i}^{v_b} \mathbf{b}_{i,d}(t) + R_{1b} \sum_{i=1}^n \mathbf{p}_i^{i_b} \mathbf{b}_{i,d}(t) \right] \sum_{j=1}^{n_\alpha} \mathbf{p}_j^\alpha \mathbf{b}_{j,d_\alpha}(t) = \\ &= \sum_{i=1}^n \sum_{j=1}^{n_\alpha} (\mathbf{p}_i^{v_b} + R_{1b} \mathbf{p}_{k,i}^{i_b}) \mathbf{p}_j^\alpha \mathbf{b}_{i,j,d}(t) \end{aligned} \quad (\text{A54a})$$

$$\begin{aligned} R_{1sc} |i_b(t)| &= R_{1sc} \left| \sum_{i=1}^n \mathbf{p}_i^{i_b} \mathbf{b}_{i,d}(t) \right| \leq R_{1sc} \left| \sum_{i=1}^n \mathbf{p}_i^{i_b} \mathbf{b}_{i,d}(t) \right| \sum_{j=1}^{n_\alpha} \mathbf{p}_j^\alpha \mathbf{b}_{j,d_\alpha}(t) \leq \\ &\leq R_{1sc} \sum_{i=1}^n \left| \mathbf{p}_i^{i_b} \right| \left| \mathbf{b}_{i,d}(t) \right| \sum_{j=1}^{n_\alpha} \mathbf{p}_j^\alpha \mathbf{b}_{j,d_\alpha}(t) \leq R_{1sc} \sum_{i=1}^n \left| \mathbf{p}_i^{i_b} \right| \left| \mathbf{b}_{i,d}(t) \right| \cdot \\ &\cdot \sum_{j=1}^{n_\alpha} \mathbf{p}_j^\alpha \mathbf{b}_{j,d_\alpha}(t) = \sum_{i=1}^n \sum_{j=1}^{n_\alpha} R_{1sc} \left| \mathbf{p}_i^{i_b} \right| \mathbf{p}_j^\alpha \mathbf{b}_{i,j,d}(t) \end{aligned} \quad (\text{A54b})$$

Afterwards, placing (A54a), (A54b) in (40a) and 40b we obtain:

$$\begin{aligned} v_{DC}^{min,h} &\leq \sum_{i=1}^n \sum_{j=1}^{n_\alpha} (\mathbf{p}_i^{v_b} + R_{1b} \mathbf{p}_i^{i_b}) \mathbf{p}_j^\alpha \mathbf{b}_{i,j,d}(t) - \sum_{i=1}^n \sum_{j=1}^{n_\alpha} R_{1sc} \left| \mathbf{p}_i^{i_b} \right| \mathbf{p}_j^\alpha \mathbf{b}_{i,j,d}(t) \leq \\ &\leq \sum_{i=1}^n \sum_{j=1}^{n_\alpha} [\mathbf{p}_i^{v_b} + R_{1b} \mathbf{p}_i^{i_b} - R_{1sc} \left| \mathbf{p}_i^{i_b} \right|] \mathbf{p}_j^\alpha \mathbf{b}_{i,j,d}(t), \end{aligned} \quad (\text{A55a})$$

$$\begin{aligned} v_{DC}^{max,h} &\geq \sum_{i=1}^n \sum_{j=1}^{n_\alpha} (\mathbf{p}_i^{v_b} + R_{1b} \mathbf{p}_i^{i_b}) \mathbf{p}_j^\alpha \mathbf{b}_{i,j,d}(t) + \sum_{i=1}^n \sum_{j=1}^{n_\alpha} R_{1sc} \left| \mathbf{p}_i^{i_b} \right| \mathbf{p}_j^\alpha \mathbf{b}_{i,j,d}(t) \geq \\ &\geq \sum_{i=1}^n \sum_{j=1}^{n_\alpha} [(\mathbf{p}_i^{v_b} + R_{1b} \mathbf{p}_i^{i_b}) + R_{1sc} \left| \mathbf{p}_i^{i_b} \right|] \mathbf{p}_j^\alpha \mathbf{b}_{i,j,d}(t). \end{aligned} \quad (\text{A55b})$$

where $\kappa - d + 1 \leq i, j \leq \kappa$.

References

1. Meng, L.; Sanseverino, E.R.; Luna, A.; Dragicevic, T.; Vasquez, J.C.; Guerrero, J.M. Microgrid supervisory controllers and energy management systems: A literature review. *Renewable and Sustainable Energy Reviews* **2016**, *60*, 1263–1273.
2. Ma, J.; Yuan, L.; Zhao, Z.; He, F. Transmission loss optimization-based optimal power flow strategy by hierarchical control for DC microgrids. *IEEE Transactions on Power Electronics* **2016**, *32*, 1952–1963.
3. Gamarra, C.; Guerrero, J.M. Computational optimization techniques applied to microgrids planning: A review. *Renewable and Sustainable Energy Reviews* **2015**, *48*, 413–424.
4. Iovine, A.; Siad, S.B.; Damm, G.; De Santis, E.; Di Benedetto, M.D. Nonlinear control of a DC microgrid for the integration of photovoltaic panels. *IEEE Transactions on automation science and engineering* **2017**, *14*, 524–535.
5. Wei, C.; Fadlullah, Z.M.; Kato, N.; Stojmenovic, I. On optimally reducing power loss in micro-grids with power storage devices. *IEEE Journal on Selected Areas in Communications* **2014**, *32*, 1361–1370.
6. Feng, K.; Liu, C.; Song, Z. Hour-ahead energy trading management with demand forecasting in microgrid considering power flow constraints. *Energies* **2019**, *12*, 3494.
7. Nahata, P.; La Bella, A.; Scattolini, R.; Ferrari-Trecate, G. Hierarchical Control in Islanded DC Microgrids with Flexible Structures. *arXiv preprint arXiv:1910.05107* **2019**.
8. Vazquez, N.; Yu, S.S.; Chau, T.K.; Fernando, T.; Iu, H.H.C. A Fully Decentralized Adaptive Droop Optimization Strategy for Power Loss Minimization in Microgrids With PV-BESS. *IEEE Transactions on Energy Conversion* **2018**, *34*, 385–395.

9. Sanseverino, E.; Di Silvestre, M.; Badalamenti, R.; Nguyen, N.; Guerrero, J.; Meng, L. Optimal power flow in islanded microgrids using a simple distributed algorithm. *Energies* **2015**, *8*, 11493–11514.
10. Zafeiratou, I.; Prodan, I.; Lefèvre, L.; Piétrac, L. Meshed DC microgrid hierarchical control: A differential flatness approach. *Electric Power Systems Research* **2020**, *180*, 106–133.
11. Fliess, M.; Lévine, J.; Martin, P.; Rouchon, P. Differential flatness and defect: an overview. Workshop on Geometry in Nonlinear Control, Banach Center Publications, Warsaw, 1993.
12. Lyche, T.; Manni, C.; Speleers, H. Foundations of spline theory: B-splines, spline approximation, and hierarchical refinement. In *Splines and PDEs: From Approximation Theory to Numerical Linear Algebra*; Springer, 2018; pp. 1–76.
13. Prodan, I.; Stoican, F.; Louembet, C. Necessary and sufficient LMI conditions for constraints satisfaction within a B-spline framework. 2019 IEEE 58th Conference on Decision and Control (CDC). IEEE, 2019, pp. 8061–8066.
14. Zafeiratou, I.; Prodan, I.; Lefèvre, L.; Piétrac, L. Dynamical modelling of a DC microgrid using a port-Hamiltonian formalism. *20th World Congress France* **2018**, *51*, 469–474.
15. Cook, M.D.; Trinklein, E.H.; Parker, G.G.; Robinett, R.D.; Weaver, W.W. Optimal and Decentralized Control Strategies for Inverter-Based AC Microgrids. *Energies* **2019**, *12*, 3529.
16. Duindam, V.; Macchelli, A.; Stramigioli, S.; Bruyninckx, H. *Modeling and control of complex physical systems: the port-Hamiltonian approach*; Springer Science & Business Media, 2009.
17. Paynter, H.M. *Analysis and design of engineering systems*; MIT press, 1961.
18. Karnopp, D.C.; Margolis, D.L.; Rosenberg, R.C. *System dynamics: modeling, simulation, and control of mechatronic systems*; John Wiley & Sons, 2012.
19. Crocker, T.R. Power converter and method for power conversion, 2005. US Patent 6,914,420.
20. Suryawan, F. Constrained Trajectory Generation and Fault Tolerant Control Based on Differential Flatness and B-splines. PhD thesis, School of Electrical Engineering and Computer Science, The University of Newcastle, Australia, 2012.
21. Löfberg, J. YALMIP: A toolbox for modeling and optimization in MATLAB. Proceedings of the CACSD Conference. Taipei, Taiwan, 2004, Vol. 3.
22. Biegler, L.T.; Zavala, V.M. Large-scale nonlinear programming using IPOPT: An integrating framework for enterprise-wide dynamic optimization. *Computers & Chemical Engineering* **2009**, *33*, 575–582.
23. van der Schaft, A.; Jeltsema, D.; others. Port-Hamiltonian systems theory: An introductory overview. *Foundations and Trends® in Systems and Control* **2014**, *1*, 173–378.
24. Stoican, F.; Prodan, I.; Popescu, D.; Ichim, L. Constrained trajectory generation for UAV systems using a B-spline parametrization. Control and Automation (MED), 2017 25th Mediterranean Conference on. IEEE, 2017, pp. 613–618.

